Article title: Transcriptome analysis of browning human neck area adipocytes reveals strong influence by the FTO intronic SNP variant in addition to tissue and PPARγ specific regulation.

Brief Title: FTO genotype, anatomical origin and rosiglitazone determine browning involving distinct pathways

Authors:

Beáta B. Tóth Ph.D.[a], Rini Arianti M.Sc.[a,b], Abhirup Shaw M.Sc.[a,b], Attila Vámos M.Sc.[a,b], Zoltán Veréb Ph.D.[c], Szilárd Póliska Ph.D.[a], Ferenc Győry Ph.D.[d], Zsolt Bacso Ph.D.[e], László Fésüs Ph.D.[a], Endre Kristóf Ph.D.[a]

László Fésüs and Endre Kristóf contributed equally to this work.

Affiliations and full addresses:

[a] Department of Biochemistry and Molecular Biology, Faculty of Medicine, University of Debrecen, Debrecen, Hungary; H-4032, Debrecen, Egyetem Tér 1., Hungary

[b] Doctoral School of Molecular Cell and Immune Biology, University of Debrecen, Debrecen, Hungary; H-4032, Debrecen, Egyetem tér 1., Hungary

[c] Regenerative Medicine and Cellular Pharmacology Research Laboratory, Department of Dermatology and Allergology, University of Szeged, Szeged, Hungary; H-6720, Szeged, Korányi fasor 6., Hungary

[d] Department of Surgery, Faculty of Medicine, University of Debrecen, Debrecen, Hungary; H-4032, Debrecen, Móricz Zsigmond körút 22., Hungary

[e] Department of Biophysics and Cell Biology, Faculties of Medicine and Pharmacology, University of Debrecen, Debrecen, Hungary; H-4032, Debrecen, Egyetem Tér 1., Hungary

Corresponding authors

László Fésüs, Address: H-4032, Debrecen, Egyetem Tér 1., Hungary, Tel: +3652-416-432, Fax: +3652-314-989, E-mail: fesus@med.unideb.hu

Endre Kristóf, Address: H-4032, Debrecen, Egyetem Tér 1., Hungary, Tel: +3652-416-432, Fax: +3652-314-989, E-mail: kristof.endre@med.unideb.hu

Abstract

Background. Brown adipocytes, abundant in deep-neck (DN) area in humans, are thermogenic with anti-obesity potential. Although analyses of tissue samples and cell clones provided important findings, their molecular features are not fully understood. FTO pro-obesity rs1421085 T-to-C SNP shifts differentiation program towards white adipocytes in subcutaneous fat.

Methods. Human adipose-derived stromal cells were obtained from subcutaneous neck (SC) and DN fat of 9 donors, of which 3-3 carried risk-free (T/T), heterozygous or obesity-risk (C/C) FTO genotypes. They were differentiated to white and brown (long-term PPARγ stimulation) adipocytes, then global RNA sequencing was performed and differentially expressed genes (DEGs) were compared.

Findings. DN and SC progenitors had similar adipocyte differentiation potential but differed in DEGs. DN adipocytes displayed higher browning features according to ProFAT or BATLAS scores and characteristic DEG patterns revealing associated pathways which were highly expressed (thermogenesis, interferon, cytokine, retinoic acid, with *UCP1* and *BMP4* as prominent network stabilizers) or downregulated (particularly extracellular matrix remodeling) compared to SC ones. Part of DEGs in either DN or SC browning was PPARγ-dependent determining enrichment for lipid metabolism and induction of some browning genes such as *PCK1*, *CPT1B*, and *PLIN5*. Presence of the FTO obesity-risk allele suppressed the expression of mitochondrial and thermogenesis genes with a striking resemblance between affected pathways and those appearing in ProFAT and BATLAS, underlining the importance of metabolic and mitochondrial pathways in thermogenesis.

Interpretation. Among overlapping regulatory influences which determine browning and thermogenic potential of neck adipocytes FTO genetic background has a so far not recognized prominence.

Funding. European Regional Development Fund [GINOP-2.3.2-15-2016-00006]

Keywords (4-6 keywords): adipocyte browning, differential gene expression patterns, deep-neck, PPARγ, FTO obesity-risk allele

Research in Context section

Evidence before this study

Browning of white adipose tissue shifts adipocytes from energy storage white to energy expenditure beige types. The balance between the two adipocyte populations in white adipose tissue is highly determined by noncoding variants of the Fat mass and obesity-associated (FTO) locus which has the strongest association with obesity. The rs1421085 FTO risk allele results in a loss of ARID5B repression of IRX3 and IRX5 which promotes excess white adipocyte formation. Recent studies have revealed the presence of brown adipose tissues at several anatomical sites in humans including the deep-neck (DN). Tissue biopsies and brown adipocytes differentiated from immortalized clonal cell of DN origin have displayed high thermogenic potential which has been partially characterized in molecular and regulatory terms. Based on differential gene expression profiles of white and beige or brown adipocytes, ProFAT and BATLAS gene lists as tools were developed to estimate browning and thermogenic potential of tissue samples and cell populations.

Added value of this study

Ex vivo differentiated, DN derived stem cell populations, compared to those derived from subcutaneous neck fat, keep their higher browning potential displayed by phenotypic, UCP1 content and ProFAT as well as BATLAS scores. It has been revealed that characteristic gene expression profile and associated pathways of brown adipocytes are determined by partially overlapping effects of tissue site specific commitments of the stem cells, PPARγ stimulation and the FTO status of donors. The presence of FTO rs1421085 risk alleles have a strong influence, manifested during differentiation, on browning resulting in compromised expression of metabolic and mitochondrial genes as well as pathways which are decisive in thermogenesis. Furthermore, several molecular pathways could be newly linked to browning, such as highly expressed interferon, cytokine and retinoic acid mediated processes and downregulation of extracellular matrix components and modelling.

Implications of all the available evidence

Regulatory elements and pathways responsible for determining brown adipocyte and adipose tissue differentiation at specific anatomical sites are more diverse than originally thought. More knowledge of the FTO allele driven regulatory pathways in brown adipose tissue would provide possible pharmaceutical targets in obese patients, particularly those carrying the risk alleles.

Introduction

Brown and beige adipocytes play a major role in maintaining the constant core body temperature of hibernating, small and newborn animals, as well as in humans without shivering[1,2]. Their heat production is mainly mediated by UCP1, a mitochondrial carrier protein, which uncouples ATP synthesis from the respiratory chain activity[1,3]. These adipocytes also conduct effective UCP1-independent thermogenic mechanisms, such as the ATP consuming futile cycle of creatine metabolism[4-7], calcium redistribution between the endoplasmic reticulum and the cytosol[8] or through release of an enzyme, encoded by *PM20D1* gene, which produces acylated amino acids that force uncoupling[9]. The stimulation of these processes leads to increased energy expenditure that can ameliorate the energy balance during obesity and type 2 diabetes mellitus[10,11]. Therefore, we need to learn in detail how regulatory networks drive the differentiation and thermogenesis of brown and beige adipocytes, especially in humans.

In rodents, brown adipose tissue (BAT) contains classical brown adipocytes which derive from myogenic precursors, accumulate numerous small lipid droplets in a multilocular arrangement and convert glucose and fatty acids into heat mostly by the action of the constitutively expressed UCP1[1,2,12]. Beige adipocytes with similar morphologic features were also described in mice. These cells arise from mesenchymal precursors and have a common developmental origin with white adipocytes, exist in distinct thermogenic fat depots and can be induced by cold and subsequent adrenergic stimulation[2,13]. In adult humans specific adipose depots are enriched in brown adipocytes; these expanse to 1-1.5% of total body mass and are mostly found in the perirenal, deep-neck (DN) and paravertebral regions[14]. It is still unrevealed whether these thermogenic fat depots represent the classical brown or the beige type of adipocytes by origin, even after recent intense studies of DN tissue which could be compared to paired subcutaneous (SC) fat samples[15-18]. First, it was reported that supraclavicular human adipocytes possess a classical brown character[16], then data derived from tissue biopsies or clonal cell lines lead to the conclusion that they rather resemble to mouse beige adipocytes[17,19]. In parallel, multiple studies using different approaches proposed specific marker genes for these browned adipocytes that are either connected them to the classical brown or to the beige lineage[16-19]. For simplicity, in this paper the term brown is used to cover both classical and beige thermogenic adipocytes in humans.

Human brown adipocytes differentiated in distinct adipose tissues express thermogenic genes at moderate levels under unstimulated conditions[2,14]. The ratio of brown and white adipocytes is partially determined during the early differentiation of mesenchymal progenitors into adipocyte subtypes which is strongly influenced by genetic predisposition[20,21]. This can be quantified in a given tissue or cell culture sample by determining BATLAS score based on the expression of 98 brown and 21 white-specific genes, which were selected by a combined analysis of gene expression signatures in mouse brown, beige and white adipocytes and human tissue samples[22]. Similarly, browning probability can be estimated by a recently developed computational tool, ProFAT[23].

A recent genome-wide association study of body fat distribution identified 98 independent adiposity loci which could affect the appearance of thermogenic fat[24]. In a detailed study by Claussnitzer et al. it has been described that single nucleotide polymorphism (SNP) rs1421085 underlies the genetic association between fat mass and obesity-associated (FTO) locus; obesity and the presence of the C risk-allele of the FTO locus results in a cell autonomous, IRX3 and IRX5 dependent shift in the gene expression programs toward white instead of brown adipocyte with lipid-storage and decreased in thermogenesis. When the T/T risk-free genotype is carried at the rs1421085 position, the ARIDB5 repressor is able to bind to this site not allowing IRX3 and 5 expression which allows adipocyte precursors to be committed for brown differentiation[20]. IRX5 knockout mice had reduced fat mass and were protected from diet-induced fat accumulation. In addition, IRX5 knockdown increased the mitochondrial respiration in isolated murine adipocytes[25]. It was also shown that IRX3 can promote browning of white adipocytes as it directly binds to the UCP1 promoter and its rare variants are associated with human obesity risk[26].

To learn more about human adipocyte browning and attempting to through more light on unresolved or controversial issues in the regulation of thermogenesis, we decided to study neck adipocyte populations derived from primary human adipose-derived stromal cells (hASCs) instead of whole tissue samples with different cell types present or single cell clones influenced by immortalization protocols. We screened and compared global gene expression patterns by RNA sequencing of hASC-derived white and brown (in response to sustained PPARγ stimulation) differentiated adipocytes. The hASCs were isolated from paired DN and SC adipose tissue samples of nine donors, 3 of each FTO rs1421085 genotype: T/T-risk-free, T/C-

heterozygous, C/C-obesity-risk. We found that both brown and beige markers, including *UCP1*, *CKMT1A/B*[4,15], *CIDEA*[27], or *PM20D1*[6] were upregulated in DN as compared to SC adipocytes, indicating a large potential of thermogenesis in the deep depots. Novel pathways and biological processes could be linked to browning regulation comparing patterns of upregulated genes. On the other hand, dozens of genes (such as *CIDEA*, *CITED1*[28] or *PM20D1* thermogenic markers) were upregulated in response to the brown differentiation as compared to white irrespective of the anatomical origin of the hASCs. The gene expression pattern of brown adipocytes was determined to a greater extent by the anatomical origin of the hASCs from which they had been differentiated than the differentiation protocol. Surprisingly, the expression of metabolic, mitochondrial and thermogenic genes was strikingly compromised by the presence of FTO rs1421085 genotypes in the progenitors. Our results suggest that cultivated hASCs from distinct locations of the human neck still keep their differing propensity for adipocyte browning which is strongly influenced by the presence of the obesity-risk alleles at the FTO intronic locus.

Materials and Methods

Ethics statement and obtained samples, isolation and differentiation of hASCs

hASCs were isolated SC and DN adipose tissue of volunteers (BMI<29.9) aged 35–75 years who underwent a planned surgical treatment. During thyroid surgeries a pair of DN and SC adipose tissue samples was obtained to rule out inter-individual variations. Patients with known diabetes, malignant tumor or with abnormal thyroid hormone levels at the time of surgery were excluded[29]. Tissue collection was complied with the guidelines of the Helsinki Declaration and was approved by the Medical Research Council of Hungary (20571-2/2017/EKU) followed by the EU Member States' Directive 2004/23/EC on presumed consent practice for tissue collection. hASCs were isolated and cultivated; white and brown adipocytes were differentiated from hASCs according to described protocols[6,7,29,30]. Briefly, both white and brown differentiations were induced by hormonal cocktails that contain apo-transferrin (Sigma-Aldrich cat# T2252), insulin (Sigma-Aldrich cat# I9278), T3 (Sigma-Aldrich cat# T6397), dexamethasone (Sigma-Aldrich cat# D1756), and IBMX (Sigma-Aldrich cat# I5879). Later, dexamethasone and IBMX were omitted from both media. In the white cocktail hydrocortisone (Sigma-Aldrich cat# H0888) was constantly present, while the brown contained insulin at 40x higher concentration than the white. However, the major difference between the two protocols was the time interval and concentration of the administered rosiglitazone (Cayman Chemicals cat# 71740). While the white regimen contained 2 μM rosiglitazone on the first four days of the two weeks long process, the differentiating brown adipocytes were treated with the drug at 500 nM concentration between the 4th and 14th days[31,32]. The absence of mycoplasma was checked by polymerase chain reaction (PCR) analysis (PCR Mycoplasma Test Kit I/C, PromoCell cat# PK-CA91)[7,29].

Flow cytometry

To investigate the phenotype of the undifferentiated hASCs, a multiparametric analysis of surface antigen expression was performed by three-color flow cytometry using fluorochrome-conjugated antibodies with isotype matching controls. See references 7 and 33 for further details about the analysis.

RNA and DNA isolation, genotyping

RNA and DNA preparation was carried out as described previously[6,7,29,30]. Rs1421085 SNP was genotyped by qPCR using TaqMan SNP Genotyping assay (Thermo Scientific cat# 4351379) according to the Manufacturer's instructions[7].

RNA-Sequencing

To obtain global transcriptome data, high throughput mRNA sequencing analysis was performed on Illumina sequencing platform. Total RNA sample quality was checked on Agilent BioAnalyzer using Eukaryotic Total RNA Nano Kit according to the Manufacturer's protocol. Samples with RNA integrity number (RIN) value >7 were accepted for the library preparation process. Libraries were prepared from total RNA using NEBNext® Ultra™ II RNA Library Prep for Illumina (New England BioLabs, Ipswich, MA, USA) according to the manufacturer's protocol. Briefly, poly-A RNAs were captured by oligo-dT conjugated magnetic beads then the mRNAs were eluted and fragmented at 94^0C degree. First strand cDNA was generated by random priming reverse transcription and after second strand synthesis step double stranded cDNA was generated. After repairing ends, A-tailing and adapter ligation steps adapter ligated fragments were amplified in enrichment PCR and finally sequencing libraries were generated. Sequencing run were executed on Illumina NextSeq500 instrument using single-end 75 cycles sequencing.

After sequencing the reads were aligned to the GRCh38 reference genome (with EnsEMBL 95 annotation) using STAR aligner (version 2.7.0a)[34]. To quantify our reads to genes, featureCounts was used (version: 1.6.3)[35].

Subsequent gene expression analyses were performed in R (version 3.5.2). Genes with low expression values or with outlier value were removed from further analysis. Briefly, after removing the highest read value of each gene we filtered out genes with reads was less than 50 considering raw reads count. Then, to further remove outlier genes we calculated Cook's distance and filtered out genes with Cook's distance higher than 1. After filtering out the low-expressed and outlier ones, the expression profile of 22362 transcripts could be examined. PCA analysis did not show any batch effect, considering sequencing date, the donor origin, and the donor sex or tissue origin. Differential expression analysis was performed using DESeq2 algorithm (version

1.22.2). When Tissue origin and differentiation protocol based differential expression was determined donor origin was controlled to decrease the effect of biological variance on thermogenic capacity[36]. However, when comparison was based on the FTO obesity-risk allele presence, we did not control donor origin. Significantly differentially expressed genes (DEGs) were defined based on adjusted P values <0.05 and log2 fold change threshold >0.85.

Hierarchical cluster analyses and heat-map visualization was performed on the Morpheus web tool (https://software.broadinstitute.org/morpheus/) using Pearson correlation of rows and columns and complete linkage based on calculated z-score of DESeq normalized data after log2 transformation. The z-score was calculated in two ways: to eliminate the donor background we calculated it by donors, or to examining FTO obesity-risk allele presence-based donor differences we determined it by considering all samples, as indicated at the figures. The interaction network and significantly enriched pathways (Reactome and KEGG or Biological processes) were determined by STRING (https://string-db.org). Edges represent protein-protein interactions. To identify Interaction network we took consideration of Textmining, Databases and Experiments based evidences from the STRING database and interaction strength score threshold was 0.4. Further analyzes of the STRING network data was performed in igraph R to identify betweenness score and bridges numbers of the interacting nodes. Different interaction thresholds (0.4-0.7) were used to visualize the network, as indicated in the figures, to obtain the interpretable complexity of the network. Interactomes were also constructed by Gephi which visualizes the fold change of the genes. Prediction of browning capacity was performed using PROFAT (http://ido.helmholtz-muenchen.de/profat/) and BATLAS (http://green-l-12.ethz.ch:3838//BATLAS/) computational tools.

Antibodies and immunoblotting

Lysis of differentiated adipocytes, denaturation, SDS-PAGE and blotting were performed as described previously. For overnight, membranes were probed at 4ºC with primary antibodies: polyclonal anti-UCP1 (1:500, Sigma-Aldrich Cat# U6382, RRID:AB_261838), and anti-actin (1:10000, Sigma-Aldrich Cat# A2066, RRID:AB_476693) in TBS-T containing 1 % non-fat skimmed milk, followed by the incubation with horseradish-peroxidase-conjugated anti-rabbit secondary antibody (Sigma-Aldrich Cat# A1949, RRID:AB_257959) for 1 hour at room

temperature. Immunoreactive proteins were visualized by Immobilion western chemiluminescence substrate (Merck-Millipore cat# WBKLS0500)[7].

Immunofluorescence staining, quantification of browning

hASCs were plated and differentiated on Ibidi eight-well μ-slides; vital and immunofluorescence staining was carried out as described previously[6,7,29,30]. Sample scanning was done by iCys Research Imaging Cytometer (iCys, Thorlabs Imaging Systems, Sterling, VA, USA). The images were processed and analyzed by our high-throughput automatic cell-recognition protocol using the iCys companion software (iNovator Application Development Toolkit version 7.0, CompuCyte Corporation, Westwood, MA, USA), Cell Profiler and Cell Profiler Analyst (The Broad Institute of MIT, MA, USA, RRID:SCR_007358). Texture sum variance and median Ucp1 protein content of adipocytes (as compared to SC white adipocytes) per cell was determined. In every experiment, 2000 cells per each sample were recorded and measured. See references 7, 30 and 37 for further details about the analysis.

Determination of cellular oxygen consumption (OC) and extracellular acidification rate (ECAR)

OC and ECAR were measured using an XF96 oxymeter (Seahorse Biosciences, North Billerica, MA, USA). hASCs of donors not related to the RNA-Seq analysis were seeded and differentiated in 96-well XF96 assay plates. Baseline, dibutyril-cAMP (Sigma-Aldrich cat# D0627) stimulated, β-guanidinopropionic acid (Sigma-Aldrich cat# G6878) and oligomycin (Enzo Life Sciences cat# ALX-380-037) inhibited OC and ECAR were recorded. As a last step, cells received a single bolus dose of Antimycin A (Sigma-Aldrich cat# U8674) at 10 μM final concentration for baseline correction. The oxygen consumption rate (OCR) and ECAR was normalized to protein content and normalized readings were shown. For statistical analysis, relative OC and ECAR levels were determined comparing basal, cAMP stimulated and oligomycin inhibited (both in unstimulated and stimulated cells) OCRs/ECARs of each sample to the basal OCR/ECAR of untreated SC white adipocytes[6,7.29].

Statistical analysis

Results are expressed as the mean±s.d. for the number of donors indicated. The normality of distribution of the data was tested by Shapiro–Wilk test. In comparison of two groups two-tailed Student's t-test was used. For multiple comparisons of groups statistical significance was calculated and evaluated by two-way ANOVA followed by Tukey post-hoc test. Statistical analysis of differential expression was performed in the R programing language with DESeq[38]. Hierarchical cluster analysis during heat map generation was performed based on Pearson correlation. n values represent biological replicates. Specific details for n value are noted in each figure legend.

Results

DN and SC progenitors have similar surface markers and adipocyte differentiation potential but differ in gene expression profile

We intended to examine global gene expression patterns of hASC-derived white and brown adipocytes and undifferentiated progenitors cultivated from paired DN and SC adipose tissue biopsies. Before doing that, we aimed to validate if adipocytes differentiated for two weeks from the aforementioned hASCs isolated from four individuals have different functional properties as described in previous studies[18,39]. Basal mitochondrial respiration of DN adipocytes was significantly elevated as compared to the SC adipocytes regardless of the obtained protocol **(Supplementary Figure 1A)**. After the cells received a single bolus dose of cell permeable dibutyril-cAMP, mimicking adrenergic stimulation, we found that adipocytes which were differentiated from DN precursors were more capable to induce their respiration than the adipocytes of SC origin. A similar trend was detected when the differentiated adipocytes were treated with oligomycin that blocks the activity of ATP synthase and provides information on proton leak respiration. In parallel, basal and cAMP-stimulated extracellular acidification rates of DN adipocytes were greater in a significant degree than those of the SC ones **(Supplementary Figure 1B)**. We could also estimate, by applying the creatine analog β-GPA, the contribution of UCP1-independent creatine futile cycle to oxygen consumption[4] and found it was more pronounced in DN adipocytes **(Supplementary Figure 1C)**.

As a further characterization of the hASCs, surface antigen analysis was performed**.** There was no significant difference in the presence of hematopoietic/monocyte, fibroblast, endothelial and integrin cell surface markers between the SC and DN precursors **(Figure 1A and Supplementary Table 1)**. Less than 5% of them had CD31, CD45 and CD146 markers which excludes substantial endothelial or leukocyte contamination. Primary abdominal subcutaneous hASCs and SGBS cells which also can be differentiated to both white and brown adipocytes[9,30,37] differed in the presence of the MCAM marker CD146. CD34 expression could be only detected on the surface of hASCs originated from DN fat and on SGBS preadipocytes.

Comparing the global gene expression profile of the hASCs obtained from the two anatomical sites of nine donors, large differences were observed. Numbers 1 to 9 on corresponding figures

throughout the manuscript label individual donors from whom sample was obtained. In this comparison, 1420 genes were differentially expressed: 878 were higher in DN and 542 in SC progenitors, respectively **(Figure 1B)**. The list of most significantly enriched pathways (only 10 are shown) determines by considering the higher expressed genes is very different between the two, except the similarly high expression of genes related to extracellular matrix (ECM) regulation. The DN hASC profile was dominated by the complement and coagulation cascade, retinoid acid biosynthesis and signaling, interaction between L1 and ankyrins, and neuronal systems and hemostasis pathways. SC precursors showed characteristic enrichment for homeobox/homeodomain mediated transcription regulation, neuroactive ligand-receptor interaction, PPAR signaling, synthesis of GPI-anchor proteins, and integrin cell surface interaction pathways (**Figures 1C-F**; Italic fonts indicate enriched pathway, biological process or compounds which also appear in some comparisons of differentiated samples presented in other figures). Unexpectedly, low levels of UCP1 expression were also detected in some preadipocyte samples, and this was more pronounced in SC preadipocytes.

The DN and SC hASCs isolated from the nine independent donors were differentiated and analyzed by laser-scanning cytometry[6,7,29,30]. The efficiency of their differentiation to adipocytes defined by expression of general fat cell markers did not differ significantly by site of origin or differentiation protocol **(Figure 2A)**. The most prominent adipogenic marker genes[40] **(Supplementary Table 2)** were expressed significantly higher (except *STAT3*) in all mature adipocyte samples as compared to progenitors and were not significantly different between SC and DN adipocytes or samples differentiated with white and brown protocols. Hierarchical cluster analysis of these genes confirmed that the samples clustered into two main groups according to their differentiation status but not by tissue origin or the differentiation protocol used, suggesting that these factors had no effect on the general adipocyte differentiation efficiency of the progenitor cells **(Figure 2B)**.

Differentiated adipocytes from DN progenitors display higher browning-related gene-expression features

Next, we investigated morphology and differential transcriptomic characteristics of adipocytes differentiated from hASCs of the nine donors. Laser-scanning cytometric data clearly showed

that the DN adipocyte population, differentiated by either the white or the brown protocol, had more brown cells characterized by the appearance of UCP1 and small lipid droplets **(Figure 2C)**. To compare tissue origin and differentiation protocol-dependent transcriptional changes related to browning, recently developed computational tools ProFAT and BATLAS were applied. When the ProFAT browning gene-set[23] was used to score browning probability, browning markers were expressed higher in the DN samples irrespective of the differentiation protocol (**Figures 2D** and **E**) and appeared in distinct clusters **(Supplementary Figure 2)**. Expression of BATLAS genes visualized as heat map by hierarchical clustering **(Figure 2F)** also showed that the differentiated DN and SC samples predominantly appeared in these two main distinct clusters and within them samples were clustered based on their differentiation protocol. Interestingly, even the white differentiation protocol resulted in BATLAS defined brown cell content **(Figure 2G)** while the highest brown cell percentage appeared in DN samples with noticeable donor variance (which was apparent in ProFAT scores as well). Six out of the BATLAS browning marker genes (*UCP1*, *CPT1B*, *EHHADH*, *AKAP1*, *SOD2*, and *ACSL5*) were expressed significantly higher in differentiated DN samples **(Supplementary Figure 3)**. Interestingly, the classical brown adipocyte marker *ZIC1*[16], was lowly expressed in both DN and SC adipocytes, and its expression was significantly increased only when the SC progenitor samples were differentiated by the brown protocol; this data questions the applicability of *ZIC1* as a lineage specific, brown adipocyte marker gene.

Checking the expression of UCP1 at protein level in differentiated adipocytes we detected the highest UCP1 content in brown adipocyte samples of DN origin **(Figure 2H**) while in adipocytes of SC origin the UCP1 expression was low. Based on the above cytometric, gene expression and metabolic data it can be concluded that adipocytes differentiated from DN progenitors have greater thermogenic potential as compared to those originated from SC adipose tissue, suggesting that cultivated hASC of distinct anatomical locations maintain their different potentials for browning *ex vivo*.

Differential gene expression patterns reveal network pathways associated with higher browning potential of DN adipocytes

After establishing the higher browning potential of cell populations derived from DN, we examined the pattern of DEGs between the DN and SC samples. Considering both the white and

the brown differentiation protocol, 1049 genes were expressed differentially in matured DN adipocytes. Approximately half of these genes were already differentially expressed at preadipocyte state (272 were higher and 250 lower expressed in DN), but the other half became expressed differentially only in differentiated adipocytes (257 were higher and 270 lower expressed in DN adipocytes) **(Figures 3A** and **B)**. Relating the DEGs in mature adipocytes to how they were expressed in preadipocytes, four distinct groups could be defined. **Figure 3A** shows a global heat map representation of the expression profile in the four groups.

257 genes (Group 1) were expressed at a greater extent in differentiated DN adipocytes as compared to SC ones and this differential expression was not observed in DN versus SC preadipocytes **(Figures 1B** and **C)**. This group includes well established browning marker genes such as *UCP1*, *PRDM16*, *CKMT1A/B*, *CIDEA*, and *PM20D1* (**Supplementary Figure 3)**. In further analyses, interaction relationships among products of higher expressed genes could be revealed using the STRING computational tool which also defined enriched pathways (KEGG and REACTOM), biological processes or cell compartments (**Figures 3C** and **D**, **Supplementary Figure 4A** by Gephi). Most of the browning marker genes mentioned above appeared in a separate cluster (black square). Interestingly, signaling pathways such as interferon alpha/beta, rhodopsin-like receptors, TRAF3-dependent IRF activation pathway and cytokine-cytokine receptor interactions were predominant among DN specific clusters, whereas metabolic pathways were scarce (e.g. mineral absorption). The observed upregulation of the metallothionein pathway is often associated with the capture of harmful oxidant radicals such as superoxide and hydroxyl radicals. These significantly enriched pathways were clearly linked to differentiated DN brown cells as they did not appear in DN preadipocytes as enriched pathways when compared to SCs **(Figures 1B-D)**. We then sought to find linkers among the characteristic functional modules of the DN specific interaction network which might have the most pronounced effect on the structure of the entire interactome. We calculated the betweenness centrality scores to point out important genes that connect different functional modules and the number of bridges to learn how many modules are connected by this gene. This network analysis confirmed the key role of *UCP1* to maintain network integrity. Other genes, such as *ESR1*, *MT2A*, *LEPR2*, *IRF7*, and *AGT* may be also pivotal for the network **(Table 1A)**.

272 genes (Group 2) were expressed at a greater extent in DN as compared to SC preadipocytes and their expression remained elevated in DN adipocytes as compared to SC ones after white or

brown differentiation, presumably contributing to higher propensity to browning **(Figures 3A** and **B)**. The most affected pathways were complement and coagulation cascades, signaling by retinoid acid and interaction between L1 and ankyrins **(Figures 3E** and **F, Supplementary Figure 4B** by Gephi**)**. As expected, pathways in this group were already revealed in the analysis of higher expressed genes in DN versus SC preadipocytes (**Figures 1B-D**, Italic font: pathway also appears in preadipocyte state; Capital letters: Pathway also appears in FTO obesity-risk allele based comparison shown below). Similarly, expression of ECM and lipid metabolism genes is different in progenitors and this difference remains significant in mature adipocytes. Also, transcriptional regulation by Homeodomain/Homeobox containing transcriptional factors was tissue specific and not affected by the differentiation state. The *BMP4* gene seems to be of paramount importance for a stable network structure; its role was already established for adipogenesis, promotion of adipocyte differentiation and brown fat development where it induces UCP1 expression[41]. In addition, *CD34*, *EFNA5*, *RARB* and *ALDH1A3* genes appeared, according to betweenness and bridges scores, to have importance in this interactome network **(Table 1B)**. *TBX1*, a well-established beige marker gene[17], also appeared in this group as an important network member.

Downregulated pathways in DN adipocytes

Next, we investigated the lower expressed genes in the DN samples. 270 genes (Group 3) were downregulated in differentiated DN adipocytes but not in SCs compared to preadipocyte differences and this differential expression was not seen in the preadipocyte state; expression of some of these genes may be non-permissive for browning. STRING network and pathway analysis showed that these genes were predominantly involved in remodeling of the ECM, cell adhesion and synthesis of GPI-anchored proteins pathways **(Figures 4A** and **B, Supplementary Figure 4C** by Gephi**)**. Cytokine signaling was also highlighted as several interleukin receptors (e.g. *IL1RE*, *IL18RE*, *IL20RE*), *TGFB3* and *KIT* were expressed higher in the matured SC adipocytes **(Figures 4C** and **D)**. *COL1A1* gene played a central role in the network, but the *GPC3*, *KRT7*, *CNR1*, and *SEMA3A* were also important in sustaining a stable network structure **(Table 2A)**.

250 genes (Group 4) were expressed at a lower extent in DN preadipocytes as compared to SC and their expression remained low in the DN adipocytes as compared to SC ones after white or

brown differentiation; these genes may be part of pathways which are not permissive for browning either. ECM organization pathways had outstanding dominance among the related pathways and the repeated appearance of the GPI-anchored protein pathway (SC preadipocytes and Group 3) emphasizes the importance of glycosylphosphatidylinositol anchored membrane proteins in the formation of the SC phenotype. In addition, the transcription regulation by homeobox and homeodomain and the neuroactive ligand-receptor interaction pathways also appeared in this group **(Figures 4C** and **D, Supplementary Figure 4D** by Gephi**)**. When analyzing relationships, the *POSTN* gene was the most significant, but *RUNX2*, *NCAM1*, *GATA2*, *EDIL3*, and *PAX3* could be also important for maintaining network connectivity. Based on their network position, the *IRX1*, *IRX3*, and *GRIA3* genes expressed higher in SC adipocytes may have roles in restraining browning potential **(Table 2B)**.

Shared PPARγ mediated gene expression patterns in DN and SC adipocytes

Both ProFAT and BATLAS estimations clearly showed that SC precursor cells also reacted to browning as compared to the white differentiation protocol by upregualting brown genes. The degree of upregulaton of these genes could be similar in DN and SC adipocytes and missed when DN and SC data were compared. Therefore, we analysed genes which responded similarly to brown differentiation protocol, that is long-term rosiglitazone exposure, in SC and DN adipocytes. Indeed, out of the 217 genes responding by upregulation to brown differentiation in either DN or SC adipocytes only 40 **(Supplementary Table 3)** were also present in Groups 1 and 2 (529 genes) described above. Eighty genes were expressed higher in brown adipocytes irrespective to their anatomical origin and they displayed enrichment of the PPAR signaling pathway **(Figures 5A-C)**. Regarding the latter glycerol kinase, *PCK1*, *CPT1B* were present among BATLAS genes[22], *PLIN5* was linked to browning[42], *ANGPTL4* had not been investigated yet in this respect. In an earlier report Loft et al. claimed that browning of human adipocytes, induced by PPARγ stimulation by rosiglitazone of stem cells isolated from prepubic fat pad of a 4-month-old male donor, required the metabolic regulator Kruppel-like factor 11 (KLF11) and reprogramming of a PPARγ super-enhancer[43]. We found that *KLF11* was among the rosiglitazone upregulated genes **(Figure 5D)** in either SC or DN adipocytes suggesting that it may be involved in the regulation of browning of neck area adipocytes.

Among the upregulated browning genes outside of the PPAR pathway, *CIDEA* was listed by ProFAT and also found in the Group 1 genes above, similarly to *PM20D1* which was strongly influenced by natural genetic variations in humans[44] and *CPT1B* which was essential for beta-oxydation of fatty acids. Gamma-butyrobetaine dioxygenase (BBOX1) catalyzes the formation of L-carnitine from gamma-butyrobetaine and has been reported to play a role in adipocyte browning[45]. The beige marker *CITED1* is a transcriptional coactivator of the p300/CBP-mediated transcription complex[28]. Higher expression of glycerol phosphate acyltransferase (GPAT3) in SC and DN brown adipocytes reflects increased triacyglicerol synthesis capacity. The mitochondrial membrane transporter for long-chain fatty acids (SLC27A3) was also upregulated in response to PPARγ stimulation. There were several other highly upregulated genes (e.g. *OAS*, *CD96*, *KRT79*) which should be investigated in the future for their possible role in brown adipocyte function. Altogether, these data shows that in addition to DN anatomical location browning potential is also determined by the appearance of PPARγ ligands in both SC and DN adipocytes.

The browning protocol also downregulated a large number of genes in either DN and SC preadipocytes and 35 overlap with Groups 3 and 4 **(Supplementary Table 4)**. Out of the downregulated genes 70 were downregulated in cells from both DN and SC origin with indication of the importance of glutathione and arachidonic acid metabolism pathways **(Figures 5E** and **F)**.

Presence of the FTO obesity-risk alleles significantly influences browning gene expression profiles

In addition to the effect of tissue localization and signaling sensitivity of hASC precursors to PPARγ, it was also examined whether the presence of the SNP rs1421085 described in the intronic region of the FTO gene could influence the thermogenic activity of adipocytes. Donor selection were based on the presence of FTO obesity-risk SNP of the FTO locus, so donors 1 to 3, 4 to 6 and 7 to 9 carried a T/T risk-free, a T/C heterozygous or a C/C obesity-risk genotype, respectively. ProFAT analysis of the expression profile of white and browning marker genes revealed that 11 browning marker genes were significantly lower (*ACAA2*, *SLC25A20*, *ACO2*, *HADHB*, *ETFDH*, *SDHB*, *NDUFS1*, *ACADS*, *DLD*, *ETFB*, *PDHA1*) and two white markers (*ALCAM*, *HOXC8*) were significantly higher expressed in FTO C/C obesity-risk genotype (**Figure 6A**, red rectangle). Evaluation by BATLAS further highlighted FTO obesity-risk allele

dependent differences, as 23 of the genes were significantly lower expressed in samples carrying the FTO C/C obesity-risk allele, while a white marker gene was expressed significantly higher in these samples (**Figure 6B**, red rectangle). Hierarchical cluster analyses based on Pearson correlation showed that 91% of the FTO T/T donor samples clustered together and 83% of the FTO C/C obesity-risk donor samples appeared in the same main cluster and they were closer to the preadipocytes considering ProFAT genes **(Supplementary Figure 5A)**. BATLAS genes assembled very similarly, 75% of the FTO T/T and 83% of the FTO C/C donor samples clustered in the same main groups and FTO obesity-risk samples appeared closer to the non-thermogenic preadipocytes. Heterozygous samples appeared in either the FTO T/T or the C/C group **(Supplementary Figure 5B)**. The ProFAT and BATLAS data clearly suggest that hASCs which carry the FTO C/C obesity-risk genotype have significantly lower browning potential.

As a next step, we investigated all the DEGs based on the presence of the FTO obesity-risk allele in the white and brown differentiated DN and SC samples and 1295 DEGs were identified. The expression of 624 and 671 genes was significantly lower or higher, respectively, in the adipocytes which carried the risk alleles as compared to the non-risk allele carriers. The expression level of these genes was not as much influenced by the FTO status in the preadipocyte state suggesting that these genes have functional role in the matured adipocytes **(Figure 6C)**. Analysis of these 1295 DEGs revealed that 81 code mitochondrial proteins, according to the Human MitoCarta 2.0 database[46] **(Supplementary Figure 5C)**. Out of those, 16 belong to one of the mitochondrial complexes and were lowly expressed in the C/C obesity-risk genotype. Only six out of the 81 mitochondrial protein encoding genes showed higher expression in the obesity-risk genotype (*SEPT4*, *PYCR1*, *PRELID2*, *CPT1A*, *MTHFD1L*, and *FKBP10*). Actually, the expression profile of genes encoding mitochondrial proteins (1035 genes in our samples out of the 1156 genes which are present in MitoCarta 2.0 database) visualized by heat map **(Supplementary Figure 5D)** also demonstrated that the majority of the mitochondrial genes were expressed at a lower extent in samples that carried the obesity-risk genotype. The genes *CKMT1A* and *CKMT1B*, which encode key mitochondrial creatine kinases and reported to be involved in UCP1-independent thermogenesis[4], were among those being significantly less expressed in FTO obesity-risk samples. All these data underline fundamental differences in the metabolic processes and mitochondrial activity between T/T and C/C adipocytes with significant deficiency in those obtained from the FTO obesity-risk donors.

STRING analysis of the DEGs influenced by the presence of FTO obesity-risk allele revealed interaction network of gene products and significantly enriched pathways with defined biological function which, by being dysregulated or deficient, may significantly contribute to the manifestation of the obese phenotype. Among the genes that were expressed at lower levels in samples carrying the FTO obesity-risk allele, metabolic pathways were most affected including lipid metabolism, thermogenesis, carbon metabolism, oxidative phosphorylation, and degradation of certain amino acids such as valine, leucine and isoleucine **(Figures 6D** and **E)**. There was a striking resemblance between the set of network pathways negatively affected by the C/C genotype and those which were demonstrable analyzing the ProFAT and BATLAS gene products **(Figures 6H-K)**. Of the 23 KEGG significantly enriched pathways defined by ProFAT genes, 21 are also found in BATLAS, and 19 of these are defined by genes that showed suppressed expression in FTO C/C samples. While the 29 KEGG pathways defined by BATLAS genes 25 were also found in pathways determined by the lower expressed genes in C/C samples. Analyzing the Reactome pathways, we found similarly high agreement **(Supplementary Table 5A-B)**. Interactome network analysis of the lower expressed genes in FTO obesity-risk genotype suggests that under normal conditions, *DECR1* (dienoyl-CoA reductase), the chemokine *CCL2*, *LIPE*, *LDHB*, *SOD2*, and *ATP5B* and *J* are central elements in maintaining connectivity **(Table 3A)**. Genes that were linked to adipo -and thermogenesis such as *SLC2A4*, *EHHADH*, *PPARGC1A*, *CPT1B*, and *FABP4* appeared with high betweenness scores. In addition to the metabolic genes, a cytokine ligand, *CCL2*, and a receptor, *CXCR4*, also appeared as important critical components of this interactome network.

Comparing the FTO status related gene expression patterns to upregulated DEGs in DN versus SC adipocytes, we found that out of the 529 genes (Groups 1 and 2) that were significantly higher in the DN samples, 33 genes were poorly expressed in the FTO obesity-risk genotype samples **(Figure 6L** and **Supplementary Table 6)**. Pathway analysis of genes with different expression based on tissue origin and presence of the FTO obesity-risk allele revealed that different pathways dominated the two. Interferon signaling and G-protein coupled rhodopsin like receptors were the prominent DN specific pathways. The FTO C/C alleles influenced metabolic pathways, e.g. fatty acid and carbon metabolism. Nonetheless, the 33 genes with similar expression in thermogenically more potent DN and appeared downregulated in the FTO obesity-risk genotype adipocytes underline the importance of PPAR signaling, lipid metabolism pathways (*CPT1B*,

FABP3, *EHHADH*, *PLA2G4A*, *ZDHHC19*), creatine kinase activity (*CKMT1A* and *CKMT1B*), carboxylic acid metabolic processes (*HYAL1*) and sodium channel regulator activity (*SGK2*, *GPLD1*) in determining browning potential.

Since the presence of the FTO risk allele may lead to loss of restrain on the expression of genes related to thermogenesis and its regulation, we also looked for and found DEGs which showed higher expression in obesity-risk genotype samples **(Figures 6F** and **G)**. Clearly, the expression of genes related to the organization of the ECM was the most prominent upregulated pathway from this respect. This is consistent with the finding that the ECM organization pathways has high importance in restraining the thermogenic potential (see gene expression and enrichment analyses in Groups 3 and 4 above and in preadipocytes). In addition, integrin cell surface interaction, TGFB, PI3K-Akt and ras signaling also appeared among significantly enriched pathways in FTO obesity-risk samples. The network analysis clearly indicated the importance of fibronectin (*FN1* gene) for the integrity of this group of networks, but also the position and relationship of others such as *CTGF*, *BDNF*, *TGFB*, and *GLI1* **(Table 3B)**; these growth and transcription factors regulate cell proliferation, differentiation and growth and can modulate expression and activation of other growth factors to determine cell fate. Considering relationship between the DN downregulated genes and those expressed higher in C/C alleles, among the 520 genes (Groups 3 and 4) whose expression was lower in DN samples, 71 was higher in FTO obesity-risk samples **(Figure 6L** and **Supplementary Table 7)**. Again, the importance of ECM organization and, in particular, the collagen degradation and integrin cell surface interactions (*COL1A1*, *COL8A1*, *COL8A2*, *COL13A1*, *SDC1*, *ACAN*, *HAPLN1*, *ITGA11*) came into focus. By further analyses of these shared gene-sets, overexpressed pro-inflammatory cytokines and cytokine receptors (e.g. *IL11*, *IL20RA*, *IL27RA*) could be linked to less thermogenic DN adipocytes and thereby to obesity and inflammation[47]. Finally, *IRX3*, which was already described as a negative[20] and positive[26] regulator of the development of thermogenic adipocytes, was also among the genes kept lowly expressed in DN and FTO T/T adipocytes but became higher expressed in the adipocytes with the obesity-risk genotype.

Discussion

Human ASCs from distinct fat depots have the potential to undergo a browning program[14]. One of the major sites that contain active BAT in humans is located in the neck, particularly in its deep regions[14,48]. When we compared SC and DN adipocyte progenitors from human neck, the latter had greater browning potential, in accordance with previous findings[18,19,39,49]. On the other hand, SC hASCs were also able to build up a significant thermogenic competency. This was supported by gene expression, morphological and functional properties of the differentiated adipocytes. Primarily, we found 1420 DEGs when the hASCs of SC and DN origins were compared. This relatively large number of DEGs and their designated pathways suggest that the two anatomically localized tissues have cells of different character at precursor level and presumably have a specific ECM structure that is maintained *ex vivo* and after differentiation. The organization of the ECM is differently regulated: degradation processes are prominent in the SC samples, whereas in DN samples ECM reorganization and regulation of vascular development appear to be significant. The retinoid acid signaling pathway is also essential and determinant in DN cells both at progenitor and at differentiated states, whose potential role in inducing thermogenesis via increasing angiogenesis by activating VEGFA/VEGFR2 signaling have been suggested but not explored in details[50,51]. It has been also recognized that the development of the neuronal system is different at the two tissues[52] and the precursor cells may be partly responsible for this.

Many genes were already proposed to predispose cells to a higher or lower thermogenic potential at the precursor level[49,53-55]. Similarly to these results in our samples, *EBF2*, *LHX8*, *MEOX2*, *TBX15* showed higher expression in DN preadipocytes, while *HOXC8*, *HOXC9*, *DTP*, and *IGFBP3* were pronounced in SC ones[55]. Several whitening and browning predisposing marker genes identified by Xue et al.[49] were also differentially expressed in our SC and DN preadipocytes, such as *S1PR3*, *GPRC5A*, *MASP1*, *C10orf90*, *ST6GALNAC3*, and *SVIL* having higher expression in DN, whereas *COL12A1*, *SHROOM3*, *GRIK2*, and *HAPLN1* being enriched in SC precursors. However, the 26 white and 25 brown marker genes pointed out by this group are highly diverse in their function and no determining pathways can be identified from the gene set that would underpin future thermogenic activity[49]. To precisely identify thermogenic adipocyte precursor cells, more information are needed about their characteristic transcriptome, determining specific pathways and molecular processes.

Majority of the gene expression studies aiming to determine the molecular, functional and developmental differences between heat-producing brown and fat-storing white adipocytes target mature adipocytes, primarily in mice but also in humans[15-19]. Interestingly, very few overlapping confirmatory results were obtained from these types of studies. It is increasingly recognized that human and mouse-based studies cannot be directly compared due to the differences in environmental exposure and the apparent difference in body mass to body surface area, which fundamentally influences body temperature homeostasis[56,57]. Therefore, humanized mouse conditions were recently optimized to generate more conclusive results[58]. It is also difficult to directly compare tissue studies with *in vitro* cellular assays and many factors could also contribute to differences observed between cellular models (e.g.: cell origin, passage number, immortality process, media composition, etc.)[59]. Recently, two global approaches based on mouse and human experimental data have identified sets of genes (ProFAT 50 and BATLAS 119), the expression pattern of which could be used, also by us, to determine the browning potential of adipocyte cells or tissues[22,23]. Surprisingly, the number of common genes in the two lists is very small, only 17. However, it turns out that ProFAT and BATLAS gene products are actually part of very similar pathways linked to increased metabolic activity as defined by KEGG or REACTOM, suggesting that it may be more appropriate to focus on gene-defined pathways, biological processes or specific cell components for better defining adipocyte browning.

In this study, we considered three different influences (anatomical origin, PPARγ stimulation by rosiglitazone and alleles of the rs1421085 FTO locus) asking what pathways and processes they induce for increased browning. Regarding site specific gene expression, we can conclude that among the 1049 DEGs in DN versus SC samples, several classical brown and beige markers are greatly co-expressed in mature DN adipocytes, e.g. *PRDM16*, *LHX8*, *EBF2*, *TBX1*, *KCNK3*, *CITED1*, *MTUS1*. The brown markers *LHX8*[16], *PRDM16*[12,60] and *EBF2*[53,54] also showed significantly higher expression in the DN samples, and the beige marker TBX1[17] had a similar pattern. Interestingly, several well-known thermogenic markers, including *ELOVL3*[61] and *PPARGC1A*[62] were not expressed differently in SC and DN adipocytes. In addition, a few brown marker genes had higher expression in SC samples differentiated by white protocol (*DIO2*[1], *HSPB7*, *EVA1A*[63]) and *ZIC1*[16] was barely expressed in all samples. Our findings are in line with the conclusions of Jespersen et al.[18] who claimed there is an overlap signature between classical murine brown and beige marker genes in adipocytes in the DN region of adult humans.

Among the pathways identified by 1049 DEGs comparing SC and DN samples, the differential regulation of ECM organization is characteristic in adipocytes of the two origins suggesting site specific organization of the ECM, which is maintained even when the cells are differentiated *ex vivo*. In addition, signaling transmitted by class A1 rhodopsin-like receptors and interferon alpha/beta receptors, which were expressed higher in DN samples, and neuroactive ligand receptors, ras proximate 1 (RAP1) G-protein and cGMP molecules which appeared elevated in SC samples, may be critical in establishing of the different functional properties of DN and SC adipocytes. The significantly enriched interferon, cytokine and other signaling pathways in DN adipocytes suggests that the anatomical origin of the progenitors determine extrinsic factors involved in cell-cell communication rather than the metabolic properties of the browning adipocytes. There are several secreted factors which were already reported to positively influence browning in an autocrine manner[64]. Notwithstanding, despite the higher expression of *UCP1* and many other thermogenic genes in DN samples, it is unexpected finding of our study that there was no significant gene expression difference in metabolic pathways between samples from the different anatomical sites. Only lipid metabolism related genes are elevated in DN samples and this process was already apparent in DN progenitors.

We used the PPARγ-agonist, rosiglitazone, which was shown to induce browning *in vivo* and *in vitro*[9,13,29,32,65] to induce thermogenically more active adipocytes. Rosiglitazone drives browning effectively *in vitro* when it is administered late in the differentiation of adipocytes[32,43]. We found 217 genes that were upregulated either in SC or DN adipocytes in response to the brown protocol with sustained rosiglitazone treatment. Eighty of these genes (and only the PPAR signaling pathway) were significantly upregulated in the adipocytes of both origins, including *KLF11*, *TSHR*, *PDK4*, *APOL6*, *CPT1B*, and *CIDEA* that showed elevated expression in response to rosiglitazone in hMADS-derived adipocytes as well[43]. Loft et al. found that during the browning of hMADS cells, which were derived from the pelvical prepubic fat pad of a 4-month-old male, rosiglitazone induced the formation of PPARγ super-enhancers without major changes in the chromatin landscape[43]. This KLF11-dependent process resulted in the upregulation of thermogenesis-related genes. This suggests that these super-enhancers are assembled upon rosiglitazone treatment in both types of primary adipocytes from the neck; however, tissue-specific transcriptional mechanisms affect their regulatory circuits resulting higher browning features in DN adipocytes as detailed above.

A super-enhancer, which is located on an obesity-risk associated locus of the intronic region of the FTO gene, was linked to the regulation of browning in subcutaneous fat[20,25,26,66] by determining the level of IRX3 and IRX5. However, the role of IRX3 and 5 in this signaling pathway remains controversial[20,25,26]. In our study, IRX3 was significantly higher expressed in samples with the FTO obesity-risk alleles and support the negative regulatory role of its gene product in thermogenesis. Interestingly, DN adipocytes (progenitors and differentiated) had also lower expression of IRX family members, including *IRX1-3* and *5-6* as compared to SC adipocytes, irrespective to their FTO allele status. This observed gene expression pattern suggests that an FTO rs1421085 SNP-independent mechanism in DN samples suppresses IRX gene expression, which could directly influence UCP1 expression. In addition, the expression profile and pathway analysis of the 1295 DEGs, based on the absence and presence of the C/C alleles, clearly points to major difference in regulation of metabolism including mitochondrial biological processes. Out of these, 624 genes (e.g. *CKMT1A/B*, *CITED1*, *PPARGC1A/B* and *CPT1B*) were lower expressed in those adipocytes that carried the obesity-risk genotype and the enriched pathways (maintained by the normal T/T genotype) included fatty acid metabolism, thermogenesis, respiratory electron transport and the signaling by retinoic acid, which also showed DN specific appearance. Surprisingly, the enriched pathways identified by these gene expression patterns include almost entirely the pathways defined by the BATLAS and ProFAT brown marker genes **(Supplementary Table 5A-B)** which suggest that this genetic predisposition has a pivotal importance in determining thermogenic competency of adipocytes from the neck. In addition to the regulation of metabolic pathways, the organization of the ECM appears to be greatly affected by the risk alleles, along with leading to enrichment of various signaling pathways (RAP1, Ras, Hippo, Relaxin, TGF-beta, PI3-Akt). In spite of the existing 104 similarly expressed DEGs in the comparisons of FTO T/T vs C/C genotypes and DN vs SC adipocytes **(Figure 7)**, FTO genotypes define largely different gene expression pattern and pathways compared to those recognized on the basis of tissue origin.

Comparing the results of the three different analytic approach used for characterization of gene expression patterns linked to browning (by anatomical origin, PPARγ stimulation and presence of the rs1421085 FTO locus), only five transcripts (carnitine palmitoyltransferase 1B, creatine kinase mitochondrial 1B, thiamine transporter 2, family with sequence similarity 189 Member A2, and long intergenic non-protein coding RNA 2458) were expressed higher in brown

adipocytes determined by all of the three conditions. Only one gene, Collagen alpha-1(VIII) chain was significantly higher expressed in those samples that showed lower thermogenic activity **(Figure 7)**. The low number of common genes and pathways suggests that these three factors elicit significantly different responses in cells in contribution to the browning transcriptome and phenotype. Interestingly, the tissue origin resulted in about two times (2.2x) more browning related DEGs than PPARγ stimulation. It is striking that the absence or presence of the FTO obesity-risk allele results in the greatest difference in the gene expression profile (1295 genes) of the differentiated cells **(Figure 7)**. Consequently, research efforts targeting the regulatory system determined by the rs1421085 FTO locus have the potential to develop novel therapeutic approaches for increasing weight loss by thermogenesis in obese patients.

UCP1-independent energy releasing processes were recently described in adipocytes, which may provide an alternative way to reduce obesity. Our RNA sequencing data showed that *CKMT1A* and *B*, futile cycle maintaining creatine kinases[4], were expressed higher in DN as compared to SC adipocytes and less abundant in those that had an obesity-risk genotype of the rs1421085 FTO locus. *PM20D1* encodes an enzyme that catalyzes the synthesis of N-lipidated/N-fatty-acyl amino acids which function as endogenous uncouplers of mitochondrial respiration in a UCP1-independent manner[6]; it was expressed higher in DN brown adipocytes and rosiglitazone increased its the expression in both SC and DN adipocytes without influence of the FTO allele status. This specific effect of the PPARγ-agonist was observed in other studies as well[9,44].

We found several genes with enriched expression in DN as compared to SC adipocytes which have not been linked to browning so far. The product of relaxin receptor 2 (RXFP2) mediates G-protein dependent stimulation of adenylate cyclase and an increase of cAMP levels[67]. Receptor-type tyrosine-protein phosphatase N2 (PTPRN2) was shown to be required for the accumulation of insulin-containing vesicles preventing their degradation[68] and accumulation of norepinephrine, dopamine and serotonin[69]. Ephrin type-A receptor 5 (EPHA5) which has a role in regulation of insulin secretion[70] was also highly expressed in DN as compared to SC brown adipocytes. Cysteinyl leukotriene receptor 2 (CYSLTR2) was shown to induce type 2 immune response in an interleukin (IL)-33 dependent manner[71]; this response was proposed but also debated to be a positive regulator of browning in mice[72,73]. In our experiments, transcripts of both genes were enriched in DN adipocytes. Further investigations are needed to confirm the direct role of these genes in the browning process.

Acknowledgements

We thank Dr. Tibor Nagy and Dr. Zoltán Barta for his help and advice in analyzing the data, Dr. Endre Barta for reviewing the manuscript and Jennifer Nagy for technical assistance.

Funding Sources

This work was supported by the European Union and the European Regional Development Fund [GINOP-2.3.2-15-2016-00006], Ministry for Innovation and Technology in Hungary [FIKP_20428-3_2018_FELITSTRAT and EFOP-3.6.3-VEKOP-16-2017-00009] and the Hungarian Research Fund [OTKA-FK131424 and K129139]. E.K. was supported by the János Bolyai Fellowship of the Hungarian Academy of Sciences and the ÚNKP-19-4 New National Excellence Program of the Ministry for Innovation and Technology in Hungary. All of the funders had not any role in study design, data collection, data analysis, interpretation, and writing of the report.

Declaration of Interests

The authors declare no competing interests with relevance to this study.

Author Contributions

Beáta Bartáné Tóth: Conceptualization, Software, Validation, Formal analysis, Data Curation, Writing - Original Draft, Writing - Review & Editing, Visualization. **Rini Arianti:** Conceptualization, Formal analysis, Writing - Original Draft, Visualization. **Abhirup Shaw:** Investigation, Writing - Original Draft. **Attila Vámos:** Formal analysis. **Zoltán Veréb:** Investigation. **Szilárd Póliska:** Formal analysis, Investigation. **Ferenc Győry:** Methodology, Resources. **Zsolt Bacso:** Methodology, Software, Formal analysis, Writing - Review & Editing. **László Fésüs:** Conceptualization, Writing - Original Draft, Writing - Review & Editing, Supervision, Project administration, Funding acquisition. **Endre Kristóf:** Conceptualization, Investigation, Writing - Original Draft, Writing - Review & Editing, Visualization, Project administration, Funding acquisition.

References

1 Cannon B, Nedergaard J. Brown adipose tissue: function and physiological significance. *Physiol Rev* 2004; **84**:277–359.

2 Kajimura S, Spiegelman BM, Seale P. Brown and Beige Fat: Physiological Roles beyond Heat Generation. *Cell Metab* 2015; **22**:546–59.

3 Fedorenko A, Lishko PV, Kirichok Y. Mechanism of fatty-acid-dependent UCP1 uncoupling in brown fat mitochondria. *Cell* 2012; **151**:400–13.

4 Kazak L, Chouchani ET, Jedrychowski MP, et al. A creatine-driven substrate cycle enhances energy expenditure and thermogenesis in beige fat. *Cell* 2015; **163**:643–55.

5 Kazak L, Chouchani ET, Lu GZ, et al. Genetic Depletion of Adipocyte Creatine Metabolism Inhibits Diet-Induced Thermogenesis and Drives Obesity. *Cell Metab* 2017; **26**:660–71.e3.

6 Kristóf E, Doan-Xuan QM, Sárvári AK, et al. Clozapine modifies the differentiation program of human adipocytes inducing browning. *Transl Psychiatry* 2016; **6**:e963.

7 Klusóczki Á, Veréb Z, Vámos A, et al. Differentiating SGBS adipocytes respond to PPARγ stimulation, irisin and BMP7 by functional browning and beige characteristics. *Sci Rep* 2019; **9**:5823.

8 Ikeda K, Kang Q, Yoneshiro T, et al. UCP1-independent signaling involving SERCA2b-mediated calcium cycling regulates beige fat thermogenesis and systemic glucose homeostasis. *Nat Med* 2017; **23**:1454–65.

9 Long JZ, Svensson KJ, Bateman LA, et al. The Secreted Enzyme PM20D1 Regulates Lipidated Amino Acid Uncouplers of Mitochondria. *Cell* 2016; **166**:424–35.

10 Harms M, Seale P. Brown and beige fat: development, function and therapeutic potential. *Nat Med* 2013; **19**:1252–63.

11 Whittle AJ, López M, Vidal-Puig A. Using brown adipose tissue to treat obesity - the central issue. *Trends Mol Med* 2011; **17**: 405–11.

12 Seale P, Bjork B, Yang W, et al. PRDM16 controls a brown fat/skeletal muscle switch. *Nature* 2008; **454**: 961–7.

13 Petrovic N, Walden TB, Shabalina IG, Timmons JA, Cannon B, Nedergaard J. Chronic peroxisome proliferator-activated receptor gamma (PPARgamma) activation of epididymally derived white adipocyte cultures reveals a population of thermogenically competent, UCP1-containing adipocytes molecularly distinct from classic brown adipocytes. *J Biol Chem* 2010; **285**: 7153–64.

14 Leitner BP, Huang S, Brychta RJ, et al. Mapping of human brown adipose tissue in lean and obese young men. *Proc Natl Acad Sci U S A* 2017; **114**: 8649–54.

15 Svensson PA, Jernås M, Sjöholm K, et al. Gene expression in human brown adipose tissue. *Int J Mol Med* 2011; **27**: 227–32.

16 Cypess AM, White AP, Vernochet C, et al. Anatomical localization, gene expression profiling and functional characterization of adult human neck brown fat. *Nat Med* 2013; **19**:635–9.

17 Wu J, Boström P, Sparks LM, et al. Beige adipocytes are a distinct type of thermogenic fat cell in mouse and human. *Ce*ll 2012; **150**: 366–76.

18 Jespersen NZ, Larsen TJ, Peijs L, et al. A classical brown adipose tissue mRNA signature partly overlaps with brite in the supraclavicular region of adult humans. *Cell Metab* 2013; **17**: 798–805.

19 Shinoda K, Luijten IH, Hasegawa Y, et al. Genetic and functional characterization of clonally derived adult human brown adipocytes. *Nat Med* 2015; **21**: 389–94.

20 Claussnitzer M, Dankel SN, Kim KH, et al. FTO Obesity Variant Circuitry and Adipocyte Browning in Humans. *N Engl J Med* 2015; **373**: 895–907.

21 Min SY, Desai A, Yang Z, et al. Diverse repertoire of human adipocyte subtypes develops from transcriptionally distinct mesenchymal progenitor cells. *Proc Natl Acad Sci U S A* 2019; **116**: 17970–9.

22 Perdikari A, Leparc GG, Balaz M, et al. BATLAS: Deconvoluting Brown Adipose Tissue. *Cell Rep* 2018; **25**: 784–797.e4.

23 Cheng Y, Jiang L, Keipert S, et al. Prediction of Adipose Browning Capacity by Systematic Integration of Transcriptional Profiles. *Cell Rep* 2018; **23**: 3112–25.

24 Rask-Andersen M, Karlsson T, Ek WE, Johansson Å. Genome-wide association study of body fat distribution identifies adiposity loci and sex-specific genetic effects. *Nat Commun* 2019; **10**: 339.

25 Bjune JI, Haugen C, Gudbrandsen O, et al. IRX5 regulates adipocyte amyloid precursor protein and mitochondrial respiration in obesity. *Int J Obes (Lond)* 2019; **43**: 2151–62.

26 Zou Y, Lu P, Shi J, et al. IRX3 Promotes the Browning of White Adipocytes and Its Rare Variants are Associated with Human Obesity Risk. *EBioMedicine* 2017; **24**: 64–75.

27 Hallberg M, Morganstein DL, Kiskinis E, et al. A functional interaction between RIP140 and PGC-1alpha regulates the expression of the lipid droplet protein CIDEA. *Mol Cell Biol* 2008; **28**: 6785–95.

28 Sharp LZ, Shinoda K, Ohno H, et al. Human BAT possesses molecular signatures that resemble beige/brite cells. *PLoS One* 2012; **7**: e49452.

29 Kristóf E, Klusóczki Á, Veress R, et al. Interleukin-6 released from differentiating human beige adipocytes improves browning. *Exp Cell Res* 2019; **377**: 47–55.

30 Kristóf E, Doan-Xuan QM, Bai P, Bacso Z, Fésüs L. Laser-scanning cytometry can quantify human adipocyte browning and proves effectiveness of irisin. *Sci Rep* 2015; **5**: 12540.

31 Fischer-Posovszky P, Newell FS, Wabitsch M, Tornqvist HE. Human SGBS cells - a unique tool for studies of human fat cell biology. *Obes Facts* 2008; **1**: 184–9.

32 Elabd C, Chiellini C, Carmona M, et al. Human multipotent adipose-derived stem cells differentiate into functional brown adipocytes. *Stem Cells* 2009; **27**: 2753–60.

33 Sárvári AK, Veréb Z, Uray IP, Fésüs L, Balajthy Z. Atypical antipsychotics induce both proinflammatory and adipogenic gene expression in human adipocytes in vitro. *Biochem Biophys Res Commun* 2014; **450**: 1383–9.

34 Dobin A, Davis CA, Schlesinger F, et al. STAR: ultrafast universal RNA-seq aligner. *Bioinformatics* 2013; **29**: 15–21.

35 Liao Y, Smyth GK, Shi W. featureCounts: an efficient general purpose program for assigning sequence reads to genomic features. *Bioinformatics* 2014; **30**: 923–30.

36 Love MI, Huber W, Anders S. Moderated estimation of fold change and dispersion for RNA-seq data with DESeq2. *Genome Biol* 2014; **15**: 550.

37 Doan-Xuan QM, Sarvari AK, Fischer-Posovszky P, et al. High content analysis of differentiation and cell death in human adipocytes. *Cytometry A* 2013; **83**: 933–43.

38 Anders S, Huber W. Differential expression analysis for sequence count data. *Genome Biol* 2010; **11**: R106.

39 Tews D, Schwar V, Scheithauer M, et al. Comparative gene array analysis of progenitor cells from human paired deep neck and subcutaneous adipose tissue. *Mol Cell Endocrinol* 2014; **395**: 41–50.

40 Lowe CE, O'Rahilly S, Rochford JJ. Adipogenesis at a glance. *J Cell Sci* 2011; **124**: 2681–6.

41 Blázquez-Medela AM, Jumabay M, Boström KI. Beyond the bone: Bone morphogenetic protein signaling in adipose tissue. *Obes Rev* 2019; **20**: 648–58.

42 Wang H, Sreenivasan U, Hu H, et al. Perilipin 5, a lipid droplet-associated protein, provides physical and metabolic linkage to mitochondria. *J Lipid Res* 2011; **52**: 2159–68.

43 Loft A, Forss I, Siersbæk MS, et al. Browning of human adipocytes requires KLF11 and reprogramming of PPARγ superenhancers. *Genes Dev* 2015; **29**: 7–22.

44 Benson KK, Hu W, Weller AH, et al. Natural human genetic variation determines basal and inducible expression of PM20D1, an obesity-associated gene. *Proc Natl Acad Sci U S A* 2019; **116**:23232–42.

45 Simcox J, Geoghegan G, Maschek JA, et al. Global Analysis of Plasma Lipids Identifies Liver-Derived Acylcarnitines as a Fuel Source for Brown Fat Thermogenesis. *Cell Metab* 2017; **26**: 509–522.e6.

46 Calvo SE, Clauser KR, Mootha VK. MitoCarta2.0: an updated inventory of mammalian mitochondrial proteins. *Nucleic Acids Res* 2016; **44**: D1251–7.

47 Hotamisligil GS. Inflammation and metabolic disorders. *Nature* 2006; **444**: 860–7.

48 Cypess AM, Lehman S, Williams G, et al. Identification and importance of brown adipose tissue in adult humans. *N Engl J Med* 2009; **360**: 1509–17.

49 Xue R, Lynes MD, Dreyfuss JM, et al. Clonal analyses and gene profiling identify genetic biomarkers of the thermogenic potential of human brown and white preadipocytes. *Nat Med* 2015; **21**: 760–8.

50 Wang B, Fu X, Liang X, et al. Retinoic acid induces white adipose tissue browning by increasing adipose vascularity and inducing beige adipogenesis of PDGFRα+ adipose progenitors. *Cell Discov* 2017; **3**: 17036.

51 Mercader J, Ribot J, Murano I, et al. Remodeling of white adipose tissue after retinoic acid administration in mice. *Endocrinology* 2006; **147**: 5325–32.

52 Daniel H, Derry DM. Criteria for differentiation of brown and white fat in the rat. *Can J Physiol Pharmacol* 1969; **47**: 941–5.

53 Wang W, Kissig M, Rajakumari S, et al. Ebf2 is a selective marker of brown and beige adipogenic precursor cells. *Proc Natl Acad Sci U S A* 2014; **111**: 14466–71.

54 Stine RR, Shapira SN, Lim HW, et al. EBF2 promotes the recruitment of beige adipocytes in white adipose tissue. *Mol Metab* 2015; **5**: 57–65.

55 Timmons JA, Wennmalm K, Larsson O, et al. Myogenic gene expression signature establishes that brown and white adipocytes originate from distinct cell lineages. *Proc Natl Acad Sci U S A* 2007; **104**: 4401–6.

56 Zuriaga MA, Fuster JJ, Gokce N, Walsh K. Humans and Mice Display Opposing Patterns of "Browning" Gene Expression in Visceral and Subcutaneous White Adipose Tissue Depots. *Front Cardiovasc Med* 2017; **4**: 27.

57 Herz CT, Kiefer FW. Adipose tissue browning in mice and humans. *J Endocrinol* 2019; **241**: R97–R109.

58 de Jong JMA, Sun W, Pires ND et al. Human brown adipose tissue is phenocopied by classical brown adipose tissue in physiologically humanized mice. *Nat Metab* 2019; **1**:830–43.

59 Silva KR, Côrtes I, Liechocki S, et al. Characterization of stromal vascular fraction and adipose stem cells from subcutaneous, preperitoneal and visceral morbidly obese human adipose tissue depots. *PLoS One* 2017; **12**: e0174115.

60 Seale P, Kajimura S, Yang W, et al. Transcriptional control of brown fat determination by PRDM16. *Cell Metab* 2007; **6**: 38–54.

61 Tvrdik P, Asadi A, Kozak LP, Nedergaard J, Cannon B, Jacobsson A. Cig30, a mouse member of a novel membrane protein gene family, is involved in the recruitment of brown adipose tissue. *J Biol Chem* 1997; **272**: 31738–46.

62 Puigserver P, Wu Z, Park CW, Graves R, Wright M, Spiegelman BM. A cold-inducible coactivator of nuclear receptors linked to adaptive thermogenesis. *Cell* 1998; **92**: 829–39.

63 Park A, Kim WK, Bae KH. Distinction of white, beige and brown adipocytes derived from mesenchymal stem cells. *World J Stem Cells* 2014; **6**: 33–42.

64 Villarroya J, Cereijo R, Gavaldà-Navarro A, Peyrou M, Giralt M, Villarroya F. New insights into the secretory functions of brown adipose tissue. *J Endocrinol* 2019; pii: JOE–19–0295.R1.

65 Lee MJ, Jash S, Jones JEC, Puri V, Fried SK. Rosiglitazone remodels the lipid droplet and britens human visceral and subcutaneous adipocytes ex vivo. *J Lipid Res* 2019; **60**: 856–868.

66 Smemo S, Tena JJ, Kim KH, et al. Obesity-associated variants within FTO form long-range functional connections with IRX3. *Nature* 2014; **507**: 371–5.

67 Hartley BJ, Scott DJ, Callander GE, et al. Resolving the unconventional mechanisms underlying RXFP1 and RXFP2 receptor function. *Ann N Y Acad Sci* 2009; **1160**: 67–73.

68 Torii S, Kubota C, Saito N, et al. The pseudophosphatase phogrin enables glucose-stimulated insulin signaling in pancreatic β cells. *J Biol Chem* 2018; **293**: 5920–33.

69 Gomi H, Kubota-Murata C, Yasui T, Tsukise A, Torii S. Immunohistochemical analysis of IA-2 family of protein tyrosine phosphatases in rat gastrointestinal endocrine cells. *J Histochem Cytochem* 2013; **61**: 156–68.

70 Jain R, Jain D, Liu Q, et al. Pharmacological inhibition of Eph receptors enhances glucose-stimulated insulin secretion from mouse and human pancreatic islets. *Diabetologia* 2013; **56**: 1350–5.

71 Liu T, Barrett NA, Kanaoka Y, et al. Type 2 Cysteinyl Leukotriene Receptors Drive IL-33-Dependent Type 2 Immunopathology and Aspirin Sensitivity. *J Immunol* 2018; **200**: 915–27.

72 Qiu Y, Nguyen KD, Odegaard JI, et al. Eosinophils and type 2 cytokine signaling in macrophages orchestrate development of functional beige fat. *Cell* 2014; **157**: 1292–308.

73 Fischer K, Ruiz HH, Jhun K, et al. Alternatively activated macrophages do not synthesize catecholamines or contribute to adipose tissue adaptive thermogenesis. Nat Med 2017; 23: 623–30.

Figure and Table Legends

Figure 1. Characterization of subcutaneous (SC) and deep-neck (DN) progenitors. (A) Surface antigen patterns of SC and DN preadipocytes. Expression of 17 markers was determined in undifferentiated preadipocytes of 3 independent donors with T/C genotype for the rs1421085 locus in the *FTO* gene by flow cytometry. The numbers represent the percentage of positive cells. n=3 **(B)** Heat map visualization of the 1420 differentially expressed genes in preadipocytes based on tissue origin (SC vs DN); 1 to 9 labels the individual from which the sample was obtained. **(C** and **E)** Interactome maps of genes greater expressed in DN preadipocytes **(C)** and SC preadipocytes **(E)**. Edges represent protein-protein interactions; 0.7 conf. **(D** and **F)** Selected significant Enriched pathways, cell components or biological processes based on DN vs SC differentially expressed genes in preadipocytes with false discovery rate (FDR) values; Italic font: pathway also appears after differentiation **(D)** higher expressed in DN **(F)** higher expressed in SC preadipocytes; n=9 donors, 6 samples/donor.

Figure 2. The degree of differentiation and browning of subcutaneous (SC) and deep-neck (DN) adipocytes. (A) Ratio of differentiated adipocytes over total number of cells. **(B)** Heat map displaying the expression profiles of general adipocyte marker genes. **(C)** Morphological features of the adipocytes differentiated from SC and DN progenitors. Texture sum variance and median Ucp1 protein content of adipocytes (as compared to SC white adipocytes) per cell. In every experiment, 2000 cells per each sample was recorded and measured. **(D)** Browning probability predicted by ProFAT software. Based on the raw gene-expression data the browning probability of the samples were analyzed and visualized by ProFAT software. **(E)** Browning probability calculated by ProFAT software considering tissue origin and differentiation protocol. **(F)** Expression profile of adipocyte specific BATLAS marker genes in SC and DN adipose progenitors and differentiated samples. **(G)** Estimation of brown cell percentage by BATLAS online tool considering tissue origin and differentiation protocol, n=9 donor, 4 samples/donor. **(H)** Expression of UCP1 at protein level in adipocyte lysates of one representative donor detected by immunoblotting. Densitometry of immunoblots performed with samples of three independent donors. W: white differentiation protocol; B: brown differentiation protocol. 1 to 9 labels the individual from which the sample was obtained. In comparison of two groups paired two-tailed

Student's t-test, in multi-factor comparison two-way ANOVA and post hoc Tukey's test was used, *p<0.05, **p<0.01.

Figure 3. Differentially expressed genes (DEGs) in subcutaneous (SC) and deep-neck (DN) mature adipocytes. (A) Heat map shows the expression profile of 1049 DEGs in SC and DN mature adipocytes. Based on how these DEGs are expressed in preadipocytes, four distinct groups were formed (Group 1-4). 1 to 9 labels the individual from which the sample was obtained. **(B)** Venn diagram shows the DEG numbers in DN adipocytes based on DN and SC comparison at preadipocyte and differentiated adipocyte state. **(C)** Interactome map and **(D)** Selected Significantly Enriched pathways and their false discovery rate (FDR) values based on DN vs SC DEGs in Group 1; 0.4 conf. **(E)** Interactome map and **(F)** Selected significantly Enriched pathways and their FDR values in Group 2; 0.4 conf. Edges represent protein-protein interactions. Italic font: pathway also appears in preadipocyte state; Capital letters: Pathway also appears in FTO obesity-risk allele based comparison. W: white differentiation protocol; B: brown differentiation protocol.

Figure 4. Interactome maps and enriched pathways, biological processes or cellular components expressed lower in deep-neck (DN) as compared to subcutaneous (SC) adipocytes. Groups of genes were defined in Figure 3A. **(A)** Interactome map and **(B)** Selected Significantly Enriched pathways and their false discovery rate (FDR) values based on DN vs SC differentially expressed genes in Group 3; 0.4 conf. **(C)** Interactome map and **(D)** Selected significantly Enriched pathways and their FDR values in Group 4; 0.4 conf. Edges represent protein-protein interactions. Italic font: pathway also appears in preadipocyte state; Capital letters: Pathway also appears in FTO obesity-risk allele based comparison.

Figure 5. Expression of genes up- and downregulated after browning protocol in both subcutaneous (SC) and deep-neck (DN) adipocytes. (A) Heat map of the 80 upregulated genes. 1 to 9 labels the individual from which the sample was obtained. **(B** and **E)** Venn diagrams of the number of genes responding to brown differentiation in SC and DN adipocytes. **(C** and **F)** Representation of overlapping up- (80) and downregulated (70) genes, respectively, in a Gephi interactome map where size of circles is proportional to the fold change in expression values. **(D)** Expression profile of *KLF11* based on DESeq normalized RNAseq data, statistics: GLM

***p<0.001. PA: preadipocytes, W: white differentiation protocol, B: brown differentiation protocol.

Figure 6. Gene expression analyses based on the presence of FTO obesity-risk allele. (A) Heat map shows the expression profile of brown and white characteristic marker genes from ProFAT database. **(B)** Heat map visualization shows differences of brown marker genes based on BATLAS database; samples ordered; n=6. **(C)** Heat map shows the expression profile of 1295 DEGs based on the presence of FTO obesity-risk alleles in SC and DN adipose progenitors and differentiated samples. **(D** and **E)** Interactome map and selected significantly enriched pathways, biological processes or cell components and their false discovery rate (FDR) values of lower expressed genes in FTO obesity-risk allele carrier samples, 0.7 conf **(F** and **G)**. Interactome map and selected significantly enriched pathways, biological processes or cell components and their FDR values of higher expressed genes in FTO obesity-risk allele carrier samples. Edges represent protein-protein interactions. SC: subcutaneous DN: deep-neck, W: white differentiation protocol; B: brown differentiation protocol. **(H** and **I)** Interactome map and Significantly enriched pathways with their FDR values of ProFAT browning marker genes; 0.4 conf. **(J** and **K)** Interactome map and Significantly enriched pathways with their FDR values of BATLAS browning marker genes; 0.4 conf. Italic font: pathway also appears in preadipocyte state; Capital letters: Pathway also appears in FTO obesity-risk allele based comparison. **(L)** FTO genotype affected genes among the differently expressed ones in DN and SC samples. 1 to 9 labels the individual from which the sample was obtained.

Figure 7. Number of differentially expressed genes in differentiated adipocytes based on tissue origin, differentiation protocol and the presence of the FTO obesity-risk allele. (A) Venn diagram shows significantly higher expressed genes number in samples expected higher thermogenic activity, and among of these genes several were lower expressed in FTO obesity-risk genotype samples **(B)** shows significantly lower expressed genes number in samples expected higher thermogenic activity, and among of these genes many expressed higher in FTO obesity-risk genotype samples. SC: subcutaneous; DN: deep-neck.

Table 1. Betweenness centrality (BC) score and Bridges number identified based on STRING Interactome network analysis by Igrapg R and Fold Changes (FC) identified by DESeq in R of the differentially expressed genes DN vs SC comparison. Average FC when

two data were considered. **(A)** Table shows genes/proteins from Group 1; **(B)** table shows genes/proteins from Group 2. n = 9 donors

Table 2. Betweenness centrality (BC) score and Bridges number identified based on STRING Interactome network analysis by Igrapg R and Fold Changes (FC) identified by DESeq R of the differentially expressed genes DN vs SC comparison. Average FC when two data were considered. **(A)** Table shows genes/proteins from Group 3; **(B)** table shows genes/proteins from Group 4. n = 9 donors

Table 3. Protein based interactome network analyses of the differentially expressed genes identified on the basis of the presence of the FTO obesity-risk allele. (A) Table shows the 15 proteins/genes with the highest betweenness centrality (BC) score and bridges number from the interaction map based on the lower expressed genes in FTO obesity-risk samples and fold change (FC) was identified by DESeq R. (B) Table shows the 15 proteins/genes with the highest BC score and bridges number from the interaction map based on the higher expressed genes in FTO obesity-risk samples and FC was identified by DESeq R. Average FC when two data were considered. n=6 donors

Figure 1.

A

Surface antigene expression

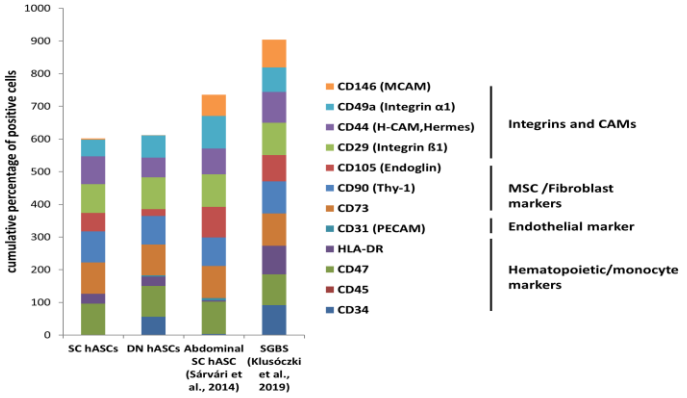

B

DEGs in SC and DN preadipocytes

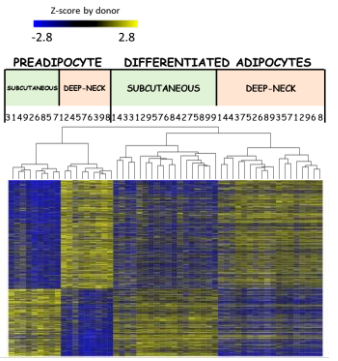

C

Interactome of higher expressed genes in DN as compared to SC preadipocytes

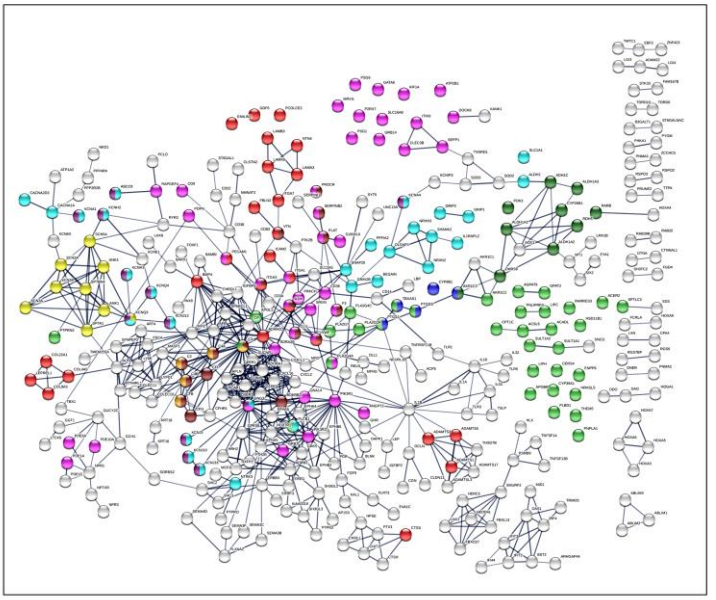

D

Enriched pathways, biological processes or components	FDR
Complement and coagulation cascades	**7.84e-0.6**
Signaling by Retinoic Acid	**0.0036**
Interaction between L1 and Ankyrins	**0.0036**
Activation of C3 and C5	**0.0053**
Extracellular matrix organization	**0.0097**
Neuronal System	**0.0115**
Hemostasis	**0.0160**
Lipid metabolism	**0.0349**
Synthesis of Prostaglandins (PG) and Thromboxanes (TX)	**0.0410**
Potassium Channels	**0.0410**

E

Interactome of higher expressed genes in SC as compared to DN preadipocytes

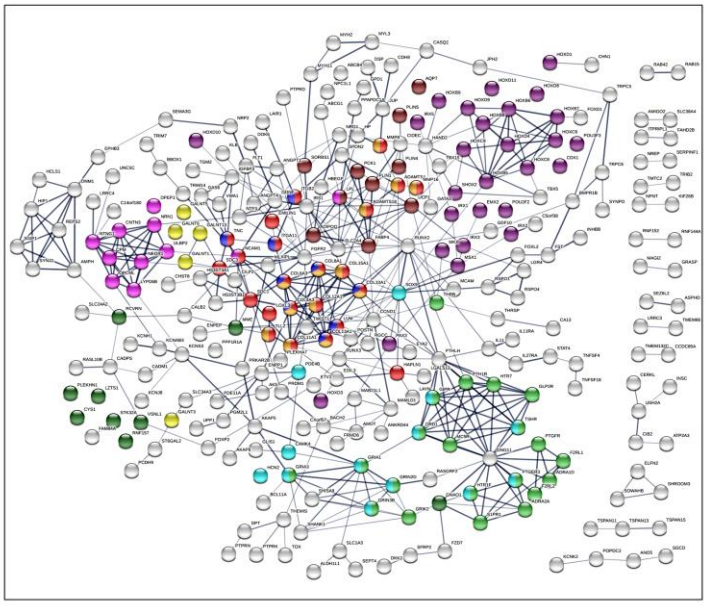

F

Enriched pathways, biological processes or components	FDR
Transcription regulation by proteins containing Homeobox/Homedomain	**1.84e-0.9**
Neuroactive ligand-receptor interaction	**0.00035**
Extracellular matrix organization	**0.00036**
PPAR signaling pathway	**0.0011**
Degradation of the extracellular matrix	**0.0046**
Post-translational modification: synthesis of GPI-anchored proteins	**0.0067**
Integrin cell surface interactions	**0.0134**
Myristate	**0.0376**
cAMP signaling pathway	**0.0411**
Mucin type O-glycan biosynthesis	**0.0439**

Figure 2.

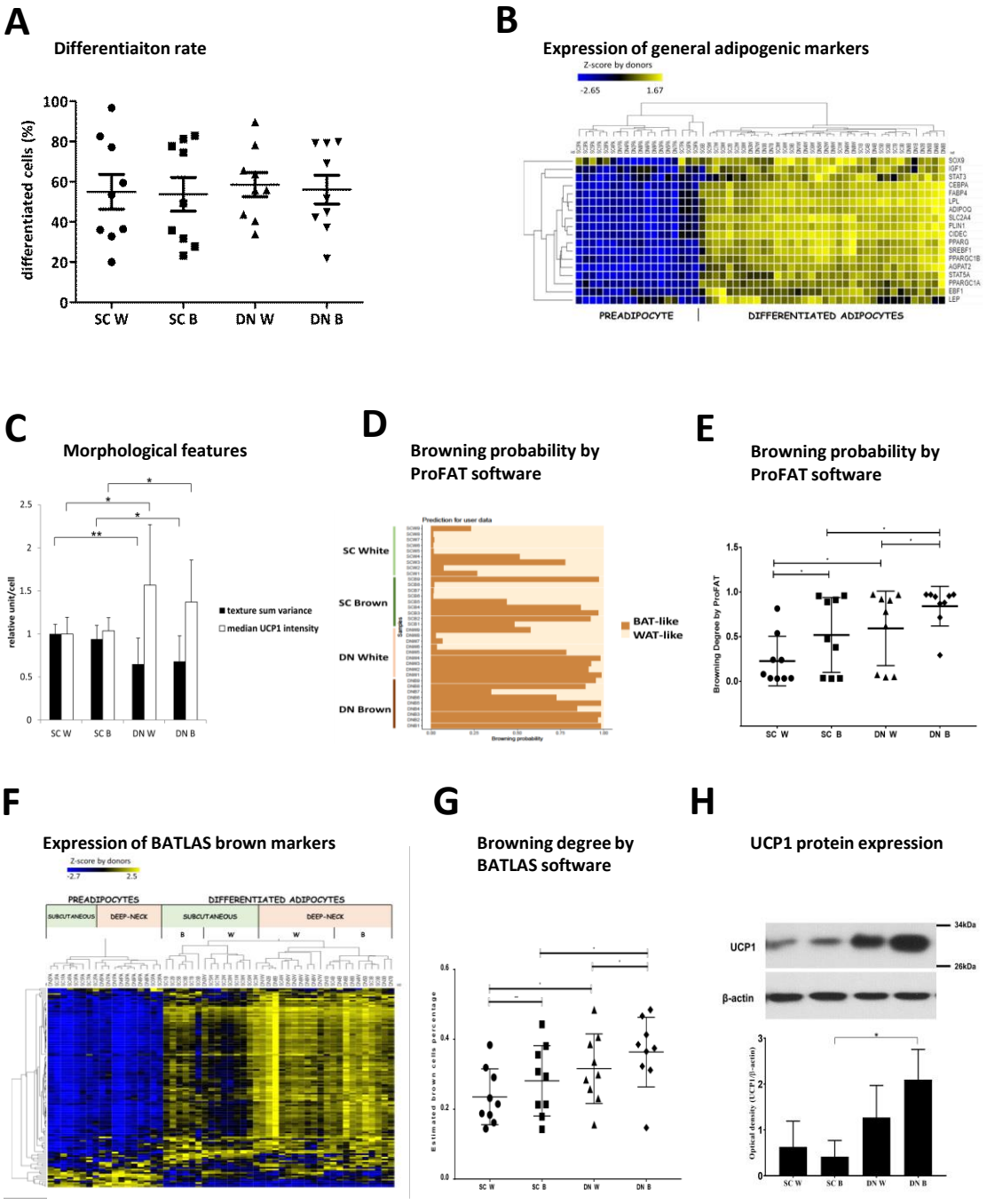
A
Differentiaiton rate
differentiated cells (%)
SC W
SC B
DN W
DN B
B
Expression of general adipogenic markers
Z-score by donors
-2.65
1.67
SOX9
IGF1
STAT3
CEBPA
FABP4
LPL
ADIPOQ
SLC2A4
PLIN1
CIDEC
PPARG
SREBF1
PPARGC1B
AGPAT2
STAT5A
PPARGC1A
EBF1
LEP
PREADIPOCYTE
DIFFERENTIATED ADIPOCYTES
C
Morphological features
relative unit/cell
texture sum variance
median UCP1 intensity
D
Browning probability by ProFAT software
Prediction for user data
SC White
SC Brown
DN White
DN Brown
BAT-like
WAT-like
Browning probability
E
Browning probability by ProFAT software
Browning Degree by ProFAT
F
Expression of BATLAS brown markers
Z-score by donors
-2.7
2.5
PREADIPOCYTES
DIFFERENTIATED ADIPOCYTES
SUBCUTANEOUS
DEEP-NECK
G
Browning degree by BATLAS software
Estimated brown cells percentage
H
UCP1 protein expression
UCP1
β-actin
34kDa
26kDa
Optical density (UCP1/β-actin)

Figure 3.

A

DEGs in SC and DN adipocytes

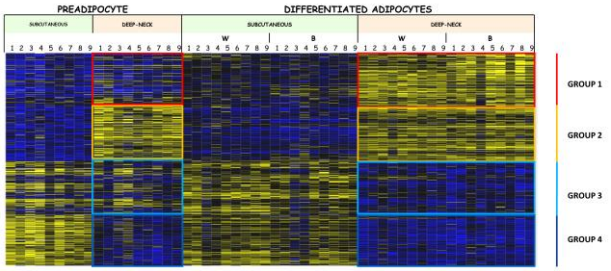

B

DEG numbers in DN adipocytes comparing with SC samples

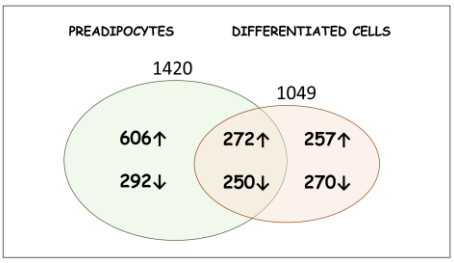

C

Interactome of Group 1 genes

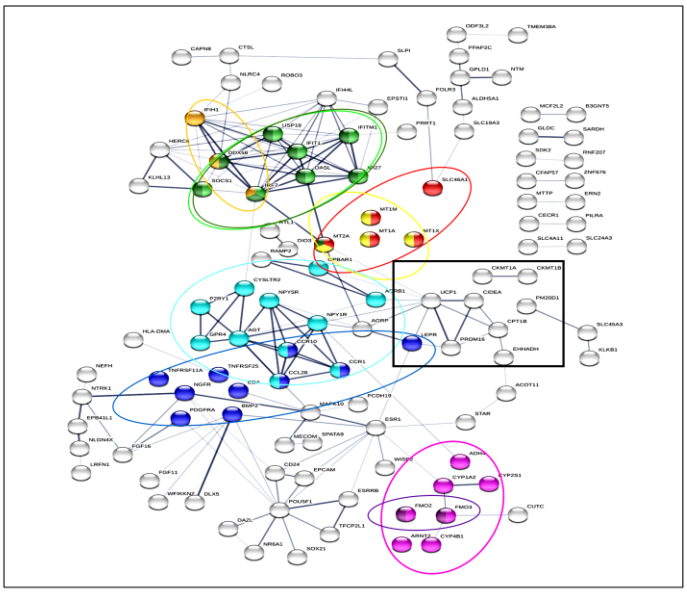

D

Enriched pathways, biological processes or components	FDR
Interferon alpha/beta signaling	0.0031
Metallothioneins bind metals	0.0031
Phase I - Functionalization of compounds	0.0126
Interferon Signaling	0.0129
Class A/1 (Rhodopsin-like receptors)	0.0251
TRAF3-dependent IRF activation pathway	0.0337
Mineral absorption	0.0427
Cytokine-cytokine receptor interaction	0.0427
FMO oxidises nucleophiles	0.0482

E

Interactome of Group 2 genes

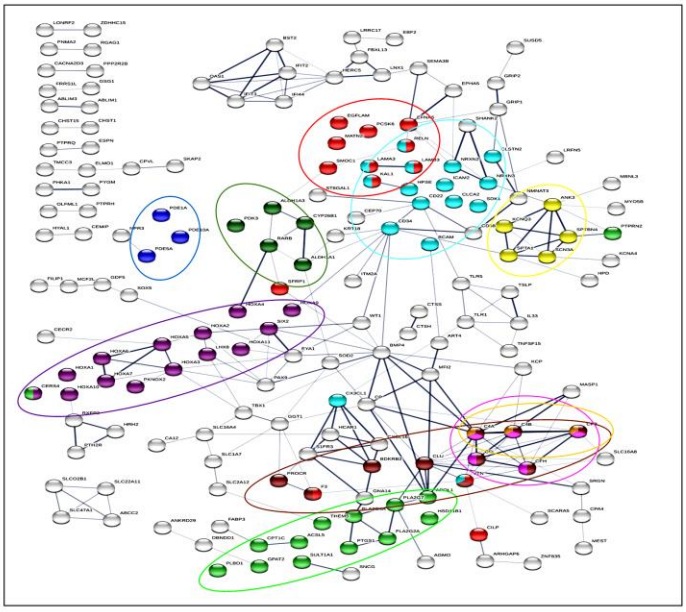

F

Enriched pathways, biological processes or components	FDR
Complement and coagulation cascades	1.22e-05
Transcription regulation by proteins contain Homeobox/Homedomain	8.80e-05
Extracellular matrix	0.0025
Cell adhesion	0.006
Interaction between L1 and Ankyrins	0.007
Lipid metabolism	0.016
Activation of C3 and C5	0.016
SIGNALING BY RETINOIC ACID	0.017
Staphylococcus aureus infection	0.039
cGMP degradation by PDEs	0.040

Figure 4.

A

Interactome of Group 3 genes

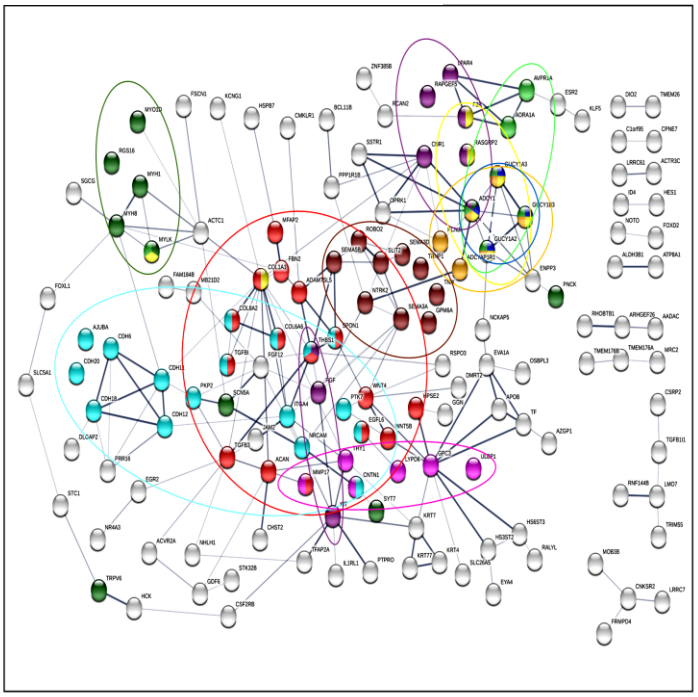

B

Enriched pathways, biological processes or components	FDR
Extracellular matrix	4.15e-06
CELL ADHESION	0.00087
Calmodulin binding	0.0189
guanylate cyclase activity, cGMP synthesis	0.0189
PLATELET ACTIVATION	0.0129
Circadian entrainment	0.0325
Vascular smooth muscle contraction	0.0325
RAP1 SIGNALING PATHWAY	0.0325
Neurogenesis	0.0320
Synthesis of GPI-anchored proteins	0.0419

C

Interactome of Group 4 genes

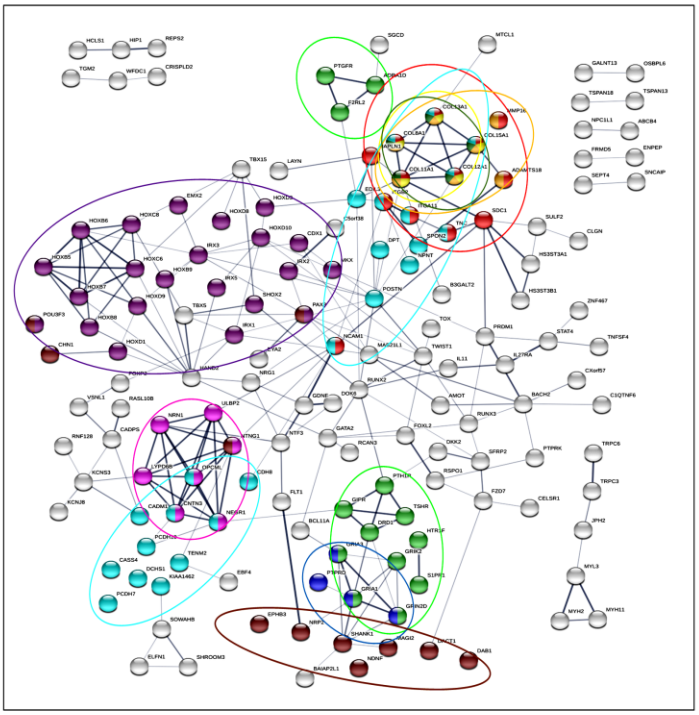

D

Enriched pathways, biological processes or components	FDR
Transcription regulation by proteins contain Homeobox/Homedomain	4.80e-12
CELL ADHESION	1.93e-08
Neuroactive ligand-receptor interaction	0.0010
Neurogenesis	0.0024
EXTRACELLULAR MATRIX ORGANISATION	0.0072
Synthesis of GPI-anchored proteins	0.0123
Collagen chain trimerization	0.0128
Synaptic adhesion-like molecules	0.0128
Degradation of the extracellular matrix	0.0481
Collagen degradation	0.0481

Figure 5.

A

80 DEGs comparing brown vs white protocols

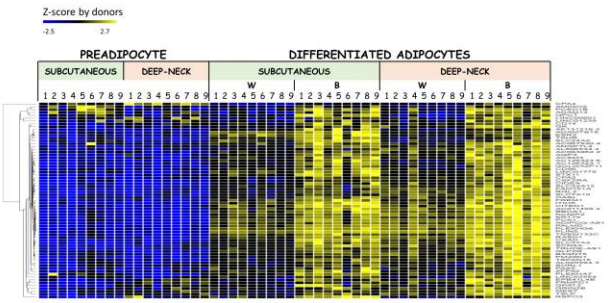

B

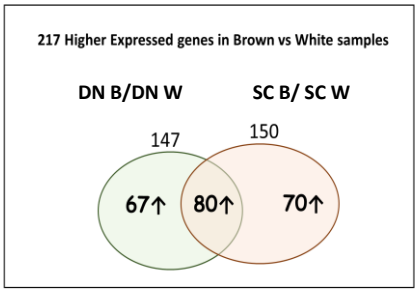

C

Interactome of 80 genes upregulated after brown protocol

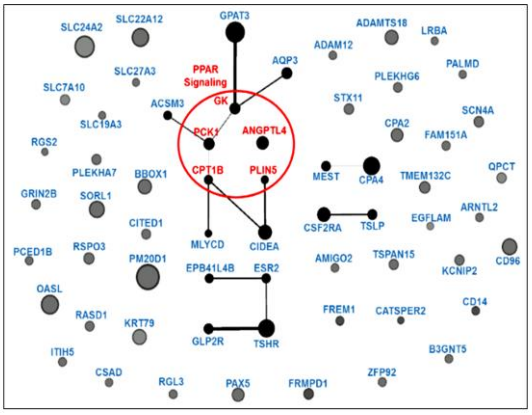

D

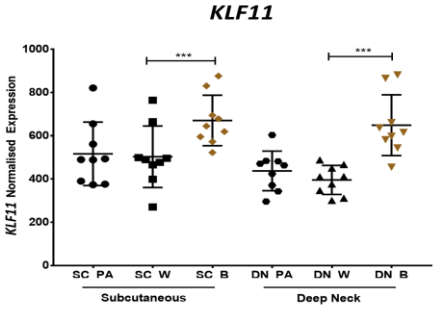

E

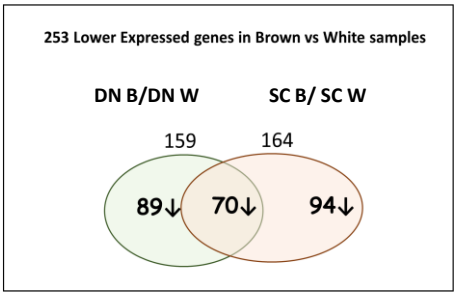

F

Interactome of 70 genes downregulated after brown protocol

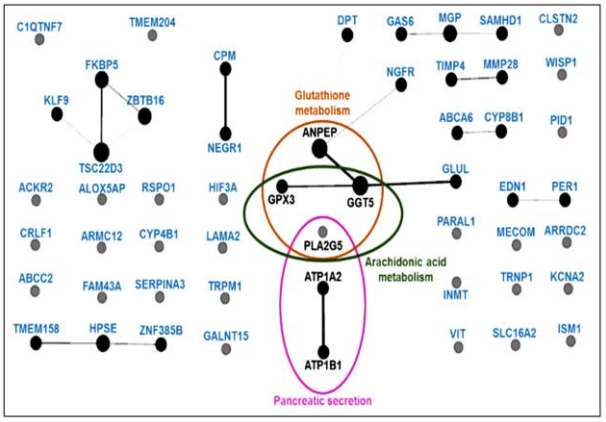

Figure 6.

A

Brown markers from ProFAT database

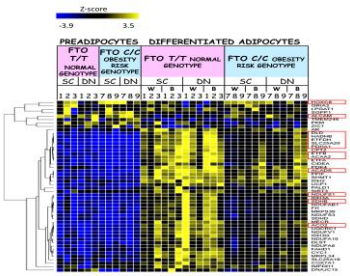

B

Brown markers from BATLAS database

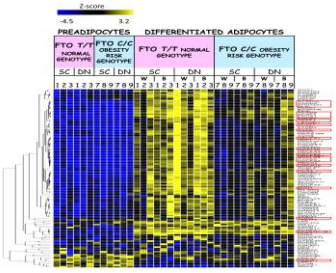

C

1295 DEGs based on the presence of *FTO* obesity-risk allele

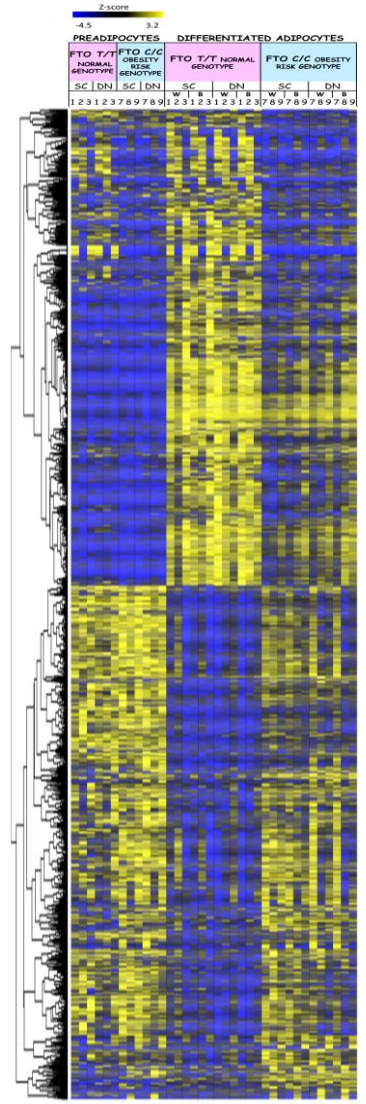

D

Interactom of less expressed genes in *FTO* obesity-risk samples

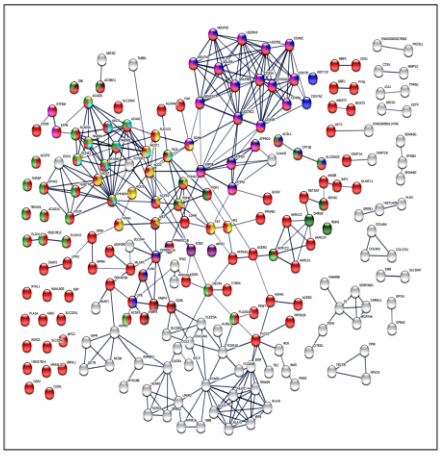

E

Enriched pathways	FDR
Metabolic Pathways	4.47e-28
Fatty acid metabolism	1.15e-13
Thermogenesis	3.88e-11
Respiratory electron transport	4.42e-11
Carbon metabolism	3.96e-10
Valin, leucine and isoleucine degradation	2.3e-06
PPAR signaling	7.01e-06
SIGNALING BY RETINOID ACID	3.49e-05
Gyoxalate and Dicarboxilate metabolism	0.00043
Mitochondrial biogenesis	0.0045

F

Interactom of higher expressed genes in *FTO* obesity-risk samples

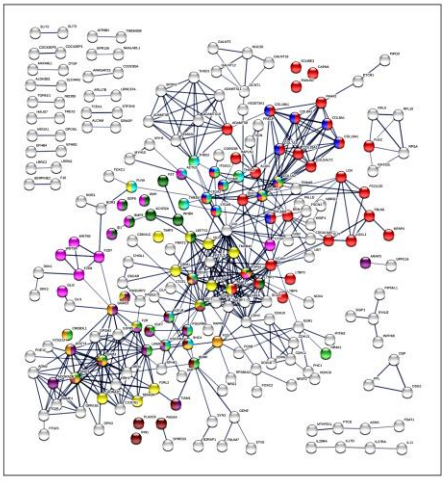

G

Enriched pathways	FDR
EXTRACELLULAR MATRIX ORGANISATION	4.5e-10
Integrin cell surface interaction	0.0007
PLATELET ACTIVATION, SIGNALING AND AGGREGATION	0.002
Focal adhesion	0.027
TGF-beta signaling pathway	0.027
PI3-Akt signaling pathway	0.027
RAP1 SIGNALING PATHWAY	0.027
Relaxin signaling pathway	0.036
Hippo signaling pathway	0.036
Ras signaling pathway	0.044

L

DEG numbers based on FTO obesity-risk allele presence and tissue origin

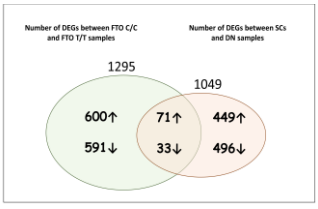

H

Brown marker genes from ProFAT database

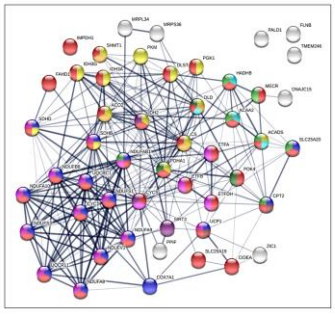

I

Enriched pathways	FDR
Metabolic Pathways	3.06e-27
Respiratory electron transport	3.73e-25
Thermogenesis	2.69e-19
Carbon metabolism	1.24e-18
Fatty acid metabolism	3.16e-06
Gyoxalate and Dicarboxilate metabolism	5.73e-06
Valin, leucine and isoleucine degradation	3.64e-05
Signaling by Retionic Acid	0.0011
Transcriptional activation of mitochondrial biogenesis	0.0018
PPAR sygnaling pathway	0.0419

J

Brown marker genes from BATLAS database

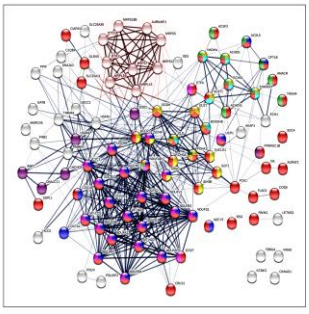

K

Enriched pathways	FDR
Metabolic Pathways	5.96e-33
Respiratory electron transport	2.20e-28
Thermogenesis	7.54e-27
Carbon metabolism	6.02e-17
Mitochondrial translation initiation	3.35e-08
Fatty acid metabolism	4.08e-08
Valin, leucine and isoleucine degradation	8.86e-08
Gyoxalate and Dicarboxilate metabolism	4.70e-07
PPAR signaling Pathway	1.70e-05
Mitochondrial biogenesis	0.00011
Signaling by Retinoid Acid	0.011

Figure 7.

A

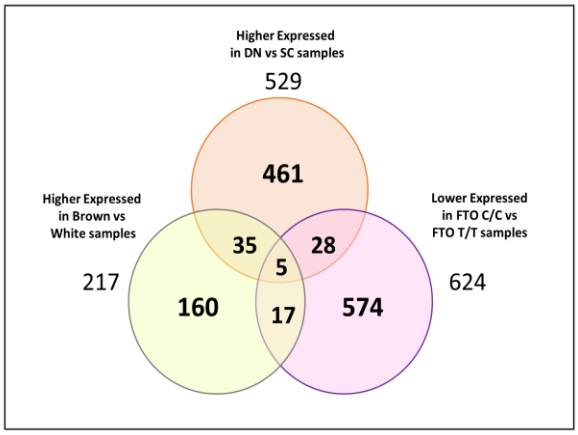
Higher Expressed
in DN vs SC samples
529
461
Higher Expressed
in Brown vs
White samples
217
35
28
5
160
17
574
Lower Expressed
in FTO C/C vs
FTO T/T samples
624

B

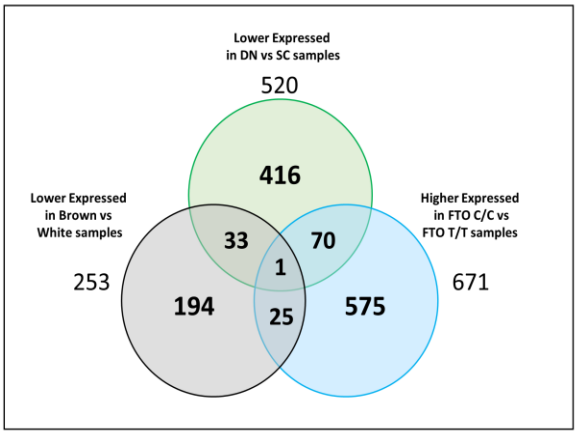
Lower Expressed
in DN vs SC samples
520
416
Lower Expressed
in Brown vs
White samples
253
33
70
1
194
25
575
Higher Expressed
in FTO C/C vs
FTO T/T samples
671

Table 1A.

Gene	BC score	Bridges	FC	Gene Description
ESR1	1445	3	2.0	estrogen receptor 1
UCP1	1323	1	6.1	uncoupling protein 1 (mitochondrial, proton carrier)
MT2A	1061	2	2.4	metallothionein 2A
LEPR	988	1	1.9	leptin receptor
IFIH1	957	0	2.0	interferon induced with helicase C domain 1
IRF7	880	2	2.0	interferon regulatory factor 7
NLRC4	864	1	1.9	NLR family, CARD domain containing 4
CTSL	813	1	1.9	cathepsin L
AGT	745	2	2.4	angiotensinogen (serpin peptidase inhibitor, clade A, member 8)
MAPK10	720	2	1.8	mitogen-activated protein kinase 10

Table 1B.

Gene	BC score	Bridges	FC	Gene Description
BMP4	2776	8	3.1	bone morphogenetic protein 4
CD34	2048	3	3.6	stem cell adhesion
EFNA5	1519	1	2.2	ephrin-A5
RARB	1362	0	3.9	retinoic acid receptor, beta
ALDH1A3	1194	1	4.4	aldehyde dehydrogenase 1 family, member A3
SMOC1	1138	1	3.2	SPARC related modular calcium binding 1
TBX1	1125	3	2.5	T-box 1
RELN	1087	0	3.1	reelin
SEMA3B	1050	1	2.2	immunoglobulin domain (semaphorin) short basic domain, secreted, 3B
SPTA1	1046	1	2.1	spectrin, alpha, erythrocytic 1 (elliptocytosis 2)

Table 2A.

Gene	BC score	Bridges	FC	Gene Description
COL1A1	2057	4	2.1	collagen, type I, alpha 1
GPC3	1113	1	3.0	glypican 3
KRT7	914	2	2.9	keratin 7
CNR1	864	1	5.8	cannabinoid receptor 1 (brain)
THY1	822	2	2.0	Thy-1 cell surface antigen
SEMA3A	781	5	2.8	immunoglobulin domain, secreted (semaphorin) 3A
FBN2	630	2	6.4	fibrillin 2
ITGA4	617	3	2.7	integrin (antigen CD49D) alpha 4 subunit of VLA-4 receptor
KCNJ6	569	0	4.2	potassium inwardly-rectifying channel, subfamily J, member 6
KIT	543	3	7.0	v-kit Hardy-Zuckerman 4 feline sarcoma viral oncogene homolog

Table 2B.

Gene	BC score	Bridges	FC	Gene Description
POSTN	1541	5	5.8	periostin, osteoblast specific factor
RUNX2	1454	5	2.9	runt-related transcription factor 2
NCAM1	1230	4	3.4	neural cell adhesion molecule 1
GATA2	1050	3	3.5	GATA binding protein 2
EDIL3	901	3	4.6	EGF-like repeats and discoidin I-like domains 3
PAX3	840	4	87.1	paired box 3
IRX1	768	3	23.4	iroquois homeobox 1
NTNG1	760	1	7.0	netrin G1
HAND2	752	2	30.5	heart and neural crest derivatives expressed 2
ITGB2	663	2	2.6	integrin, beta 2 (complement component 3 receptor)

Table 3A.

Gene	BC score	Bridges	FC	Gene Description
ATP5B	2015	18	2.2	ATP synthase beta polypeptide
SDHB	1028	18	2.0	succinate dehydrogenase complex
SUCLG1	1064	16	2.1	succinate-CoA ligase
SOD2	2418	14	2.4	superoxide dismutase 2
DECR1	7717	13	1.8	2,4-dienoyl CoA reductase 1
CD36	1730	13	2.4	Thrombospondin Receptor
ACADM	1531	13	2.2	acyl-CoA dehydrogenase
NDUFS1	200	13	1.8	NADH dehydrogenase Fe-S protein 1
MDH1	968	12	2.7	malate dehydrogenase 1
PPARGC1A	854	12	2.6	peroxisome proliferator-activated receptor gamma
UQCRC2	139	12	2.0	ubiquinol-cytochrome c reductase core protein II
ACSL1	525	11	1.8	acyl-CoA synthetase long-chain family member 1
CPT1B	294	11	2.0	carnitine palmitoyltransferase 1B
CCL2	4845	10	2.5	chemokine (C-C motif) ligand 2
LIPE	3792	10	2.6	lipase hormone sensitive

Table 3B.

Gene	BC score	Bridges	FC	Gene Description
FN1	17619	37	2.1	fibronectin 1
CTGF	5508	16	2.6	connective tissue growth factor
VCAN	1117	16	2.4	versican
TGFB1	5194	14	1.9	transforming growth factor, beta 1
COL1A1	4343	14	2.7	collagen, type I, alpha 1
CDH2	3971	14	2.6	cadherin 2, type 1, N-cadherin (neuronal)
BDNF	5515	13	2.0	brain-derived neurotrophic factor
VCAM1	3666	12	3.1	vascular cell adhesion molecule 1
TIMP1	2592	12	2.5	TIMP metallopeptidase inhibitor 1
LOX	1377	12	2.0	lysyl oxidase
VEGFC	3627	11	1.9	vascular endothelial growth factor C
FOS	2986	9	2.0	FBJ murine osteosarcoma viral oncogene homolog
SDC1	2729	9	2.4	syndecan 1
BGN	1644	9	3.9	biglycan
GLI1	5192	8	2.7	GLI family zinc finger 1